SSRG International Journal of Geo-informatics and Geological Science
ISSN: 2393 – 9206 /doi:10.14445/23939206/IJGGS-V8I2P107

Volume 8 Issue 2, 67-88, May-Aug, 2021

Original article

Trace and REEs Geochemistry, A Tool To Study Mudrocks And Quaternary Deposits Found in Babouri-Figuil Intracontinental Basin (North Cameroon): Provenance, Depositional Conditions, And Paleoclimate

Nguo Sylvestre Kanouo*[1], Aubin Nzeugang Nzeukou[2], Arnaud Patrice Kouské[3], Clarisse Tcheombé Bahané[2], Robert Kringle[4], Emmanuel Archelaus Afanga Basua[5], Nathalie Fagel[6]

[1]*Mineral Exploration and Ore Genesis Unit, Department of Mining Engineering and Mineral Processing, Faculty of Mines and Petroleum Industries, University of Maroua, 08 Kaélé, Cameroon*
[2]*Department of Earth Sciences, Faculty of Science, University of Maroua, Maroua, Cameroon*
[3]*Department of Civil Engineering, The University Institute of Technology, University of Douala, Cameroon*
[4]*Federal Institut, for Geosciences and Natural Resources (BGR) 30161 Hannover, Germany*
[5]*State Key Laboratory of Biogeology and Environmental Geology, China University 8 of Geosciences, Wuhan 430074, China*
[6] *Laboratory of Clays, Geochemistry and Sedimentary Environment, Department of Geology, University of Liège, 14B-4000 Liège, Belgium*

Received Date: 03 July 2021
Revised Date: 04 August 2021
Accepted Date: 15 August 2021

Abstract *-Trace and REEs geochemical analysis was carried out on mudrocks and fine-grained-rich Quaternary deposits from five pits dug. Results were used to chararacterize each sedimentatry formation and to determine the provenance, tectonic setting, depositional conditions, and paleoclimate. Mudrocks show relatively high Sr, Ba, Zr, and LREE contents with Sr being exceptionally high in schistose marls, which generally have the lowest Ba and Zr contents. Provenance interpretation suggests that the lithified sediments (all from Upper continental Crust) were sourced mainly from post-Archean strata. La/Th versus Hf, Co/Th versus La/Sc, and La/Yb versus ∑REE binary diagrams show continental tholeiitic basaltic, alkaline basaltic, and/or sedimentary rocks sources, with part of the later being carbonaceous. Depositional interpretations suggest that these studied lithified sediments were mainly deposited in a passive continental margin setting under oxidizing to reducing conditions. Paleoclimatic and paleosalinity analyses suggest that the climatic conditions in Babouri-Figuil during depositional periods were warm and humid, cool and arid, and warm and arid. Mudstone's and schistose marl's sediments were mainly deposited in lacustrine and marine environments, respectively.Quaternary deposits characterizations show that those from Pomla and Sorawel have relatively higher trace and REEs than those from Délélé, Kolé, and Mayo Figuil. Provenance studies suggest that the sediments were mainly originated from Upper Continental Crust, and post-Archean strata. Sediments in Délélé and Kolé were sourced from felsic, mafic, and sedimentary rocks. Those in Pomla, Sorawel, and Mayo Figuil were mainly originated from felsic rocks. Depositional interpretation, suggest that the studied sediments were deposited in a range from reducing to oxidizing conditions. Paleoclimatic interpretations suggest that Babouri-Figuil was arid and cool during deposition in Pomla and arid and warm during deposition in Délélé, Sorawel, Kole, and Mayo Figuil.*

Keywords *- Cameroon, Babouri-Figuil Basin, mudrocks, Quatenary deposits, trace and REEs, provenance, tectonic setting, deposition, paleoclimate.*

I. Introduction

A trace element in geochemistry is a chemical element whose concentration is less than 1000 ppm (0.1%) of a rock's composition, including ores, soils, sediments etc. This includes high field strength elements (HFSE), some large-ion lithophile elements (LILE), and transitional elements (TE) [1,2, 3]. Trace element geochemistry is

used to discriminate tectonic settings of igneous rocks and understand their petrogenesis (e.g., [4,5,6,7])). Other usefulness of trace element geochemistry are: to help develop a genetic model of some metamorphozed (e.g., [8,9,10]) and unmetamorphozed ore bodies (e.g.,[11,12]); and to study oil-source correlation and hydrocarbon migration (e.g., [13,14]). Trace element geochemistry is also an important tool for exploring mineable ore deposits (e.g., [8,12, 15]), crude oil deposits (e.g., [16, 17]) and environnemental assessment (e.g., [3, 18, 19, 20]). Trace element geochemistry has been applied to study sediment provenance (e.g., [21-25]) and paleoclimate (e.g.,[19, 26, 27]). It is also used to infer tectonic setting during a basin's creation (e.g., 28- 30]) and depositional conditions [31- 33]. The study of trace and REEs is therefore, very important in applied and fundamental geology.

The Babouri-Figuil Basin (Fig. 1) in the north region of Cameroon is filled with Cretaceous-aged siliciclastic and carbonate sedimentary rocks (with some organic C enrichments) [33, 34,35]. These sedimentary rocks are locally overlain Precambrian-aged metamorphic and magmatic basement rocks [36]. The sedimentary and Precambrian rocks are partially overlain by terrigenous siliciclastic sediments and supergenous soils (considered as Quaternary:[37, 38]). Less attention has been paid to these Quaternary materials, and limited published data are available for lithified sediments found in this basin. The most recent published researchs on lithified sediments in this basin are those of [33, 35, 39]. Abolo et al. [35] determine the XRD mineralogical composition of four samples from oil shales (in Mayo Figuil and Mayo Tafal, East of the basin), and used inorganic and organic geochemistry to assess economic importance. Ondoa et al. [39] used magnetic susceptibility to characterize sedimentary strata in the basin. Much still has to be done to better understand the formation history of sedimentary rocks in the Babouri-Figuil Basin. Tchouatcha et al. [33] recently present petrographic features and whole-rock geochemical results for fine grained lithified clasts sampled from lithostratigraphic colums found in the Babouri-Figuil Basin. These data were use for provenance study, to reconstitute palaeoweathering processes and to determine depositional environment. In this paper, we use trace and rare earth geochemistry to characterize mudrocks (mudstones and schistose marls) and Quaternary deposits found in the Babouri-Figuil Basin. The obtained data are also used to: (1) constrain the provenance and origin of host materials and (2) infer tectonic setting, depositional conditions, and paleoclimate.

II. Geography and Geologic settings

The Babouri-Figuil Basin found in the north region of Cameroon, is a low relief bordered in the north and south by a succession of high lands (Fig. 2). The high land topographies are mainly composed of magmatic and sedimentary rocks, ranging in height from 400 to above 800 m (Fig. 2). The height of those magmatic rocks, exceeds 400 m, whereas those made up of sedimentary rocks range in height from 300 to 400 m. The low land (below 300 m) is prodominantly sedimentatry and metamorphic rocks with the latter also found along the border of the basin.

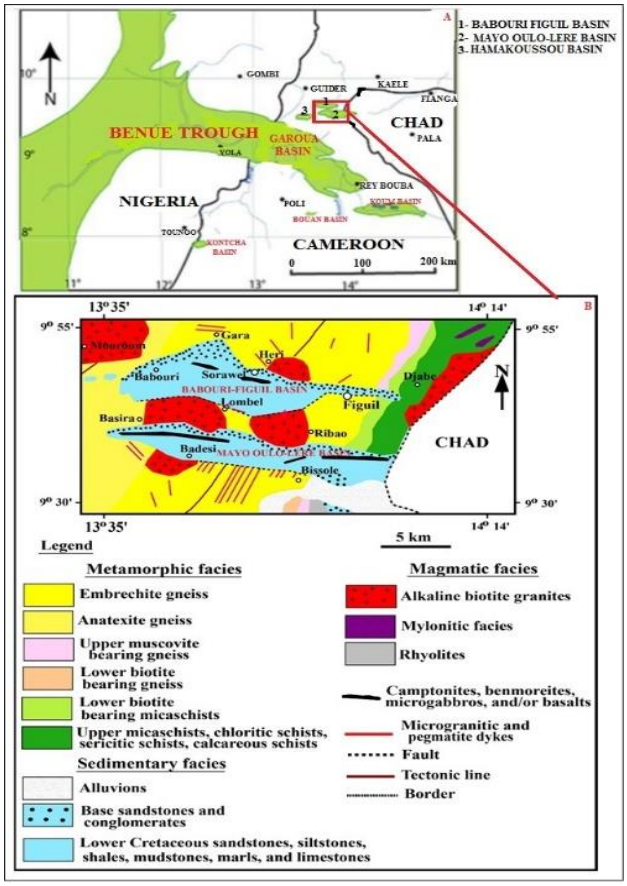

Fig. 1: Sketch geologic maps locating the area of study within the local and regional settings, adapted from [36] and modified with data from [40]

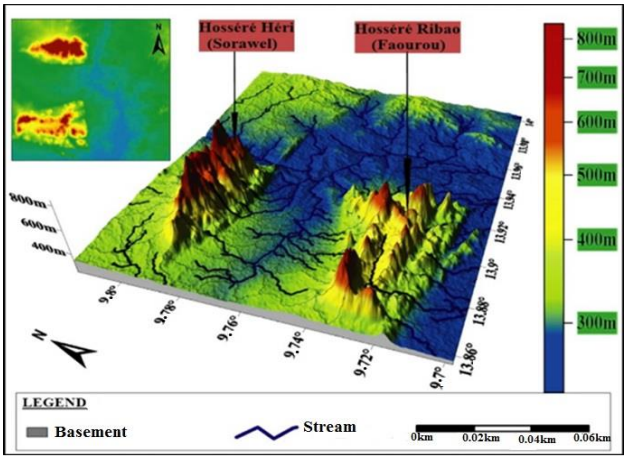

Fig. 2: 3D geomorphological map of the study area showing different topographic units

The Babouri-Figuil Basin is an intracontinental E-W tectono-sedimentary megastructure whose Cretaceous opening is suggested to be related to that of the Benue Trough found in the East of Nigeria [34]. This half-graben basin [40] is composed of : (1) metamorphic rocks; (2) magmatic rocks; (3) lithified sediments; and (4) unconsolidated sediments and well developed soils [36]. The metamorphic rocks forming the basement (part of the Cameroon mobile belt), are locally cut by numerous faults and veins, with dykes filled with felsic and/or mafic magmatic products [41, 42]. These metamorphic rocks are two generations: the very old and strongly tectonized and migmatized gneiss (covering most of the basement terrains); and old and weakly tectonized rocks found in the East (upper muscovite bearing gneiss, marbles, calc-schists, chlorite schists, sericite schists, upper mica-schists and quartzites) [36]. Migmatized gneiss was folded by NNE–SSW PanAfrican orogeny [43]. The two groups of metamorphic rocks were intruded by felsic and mafic magmas during local extension (undated). The felsic magmatic rocks (dyke-like and alkaline granitoids stocks) are medium to coarse grained and dominantly pink to reddish in colour. Mafic fractured filling dyke-like rocks are basaltic in composition.

The metamorphic and magmatic rocks are locally overlain by sandstones and conglomeratic sandstones [36]. Other rocks found in the Babouri-Figuil Basin with some local alternating units are mudstones, shales, siltstones, calcareous sandstones, calcareous marls, marls, and limestones [33, 35, 36, 39]. Part of these sedimentary rocks are cut in the north of the basin by East to West camptonite and benmoreite dykes [40]. Both sedimentary, magmatic, and metamorphic rocks are partially overlain by sediments along main streams and old stream's channels.

III. Materials and Methods

A. Sampling

Field survey and pitting were carried in the Babouri-Figuil Basin. Twenty nine (29) mudrock samples were collected from six outcrops found in Dafang (DFG), Mayo Tafal (TFL), and Mayo Figuil (MFL). Five test pits were dug in alluvial flats forming old river channels in Délélé (DLE), Pomla (PLA), Sorawel (SRL), Kolé (KLE), and Figuil (MFGL). These pits were dug at the bank of the following main streams (Mayo Délélé, Mayo Louti, Mayo Tafal, Mayo Kolé, and Mayo Figuil). Fifty (50) samples were collected from each layer of the dug pits.

B. Geochemical analyses

Fourty one samples (16 mudrocks : 6 mudstones and 10 schistose marls) and (25 fine-grained-rich intervals of pits) were sent to the laboratory to determine their trace and rare earth element compositions. These analyses were carried out by Inductively Coupled Plasma-Mass Spectrometry (ICP-MS) in the Central Africa Royal Museum in Belgium. Collected samples were dried at 120°C in drying oven overnight. Dried samples were chiped and grounded in an agate mortar to obtain fine powder before submission to ICP-MS analysis. 100-200 mg each powder was fused with $LiBO_2$ and then the glass beads were digested using dilute nitric acid. To certify data quality (95% confident level) and calibrate the equipment for optimal precision, a replicate, standard and blank was measured. The detection limits for trace and rare earth elements are the following: Sc, Sr, Ni, and Cu (0.5 ppm); V, Cr, Co, and Ba (0.2 ppm), Ga, Zr, and Rb (0.1 ppm); Ge, Cs, Nd, Ta, and W (0.05 ppm); Ce (0.04 ppm); Y, Nb, La, Pr, Sm, Gd, Hf, and Pb (0.02 ppm), Eu, Dy, Ho, Er, Yb, Th, and U (0.01 ppm); and Lu (0.002 ppm).

IV. Field Relationships

A. Mudrocks

The studied mudrocks outcrop in three zones: (1) mudstones at Dafang; (2) mudstones in Mayo Tafal; and (3) schistose marls at Mayo Figuil. Dafang mudstones are a half-dome, monoclinal (N87E27S), massive to layered, greyish to brownish-yellow mudstone successions (Fig. 3a). Mayo Tafal mudstones are a monoclinal (N87E20S : Fig. 3b) succession of layered to weakly laminated, grey to greenish-grey mudstones with local alternation of limestones layers. Schistose marls outcroping in Mayo Figuil show structural and colour variation (Figs. 3c,d). They are monoclinal (N120E75SSW), schistose, layered to laminated and locally enclose limestone bands, lenses, pockets, and veinlet cross-cuttings. Their colour ranges from greenish-grey to light grey or whitish grey. These rocks are locally overlain or alternate with dark-grey schales (oil shales:[35]).

B. Quaternary deposits

Pitted Quaternary deposits overly schistose marl at the bank of Mayo Figuil (in Figuil), mudstone at the bank of Mayo Louti (in Pomla), black shale at the bank of Mayo Tafal (in Sorawel), migmatized gneiss at the bank of Mayo Kolé (in Kole), and mica schist at the bank of Mayo Délélé (in Délélé). The textural features and organization of each pit are presented in Figs. 4 and 5.

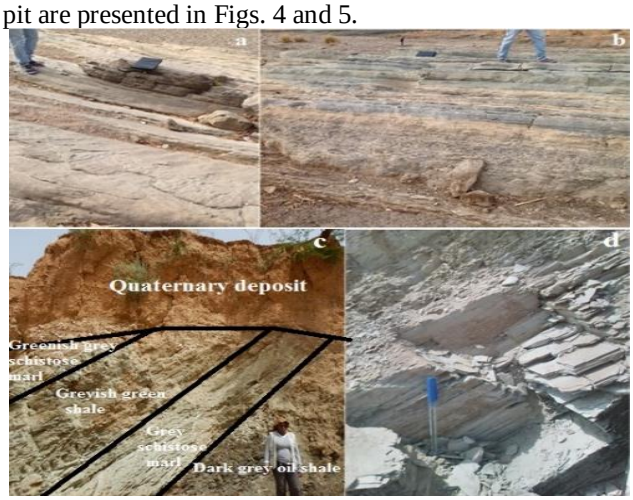

Fig. 3: Mudrock outcrops in Babouri-Figuil (a: outcrop showing Dafang mudstones; b: outcrop showing Mayo Tafal mudstones; c-d: outcrop showing Mayo Figuil schistose marls).

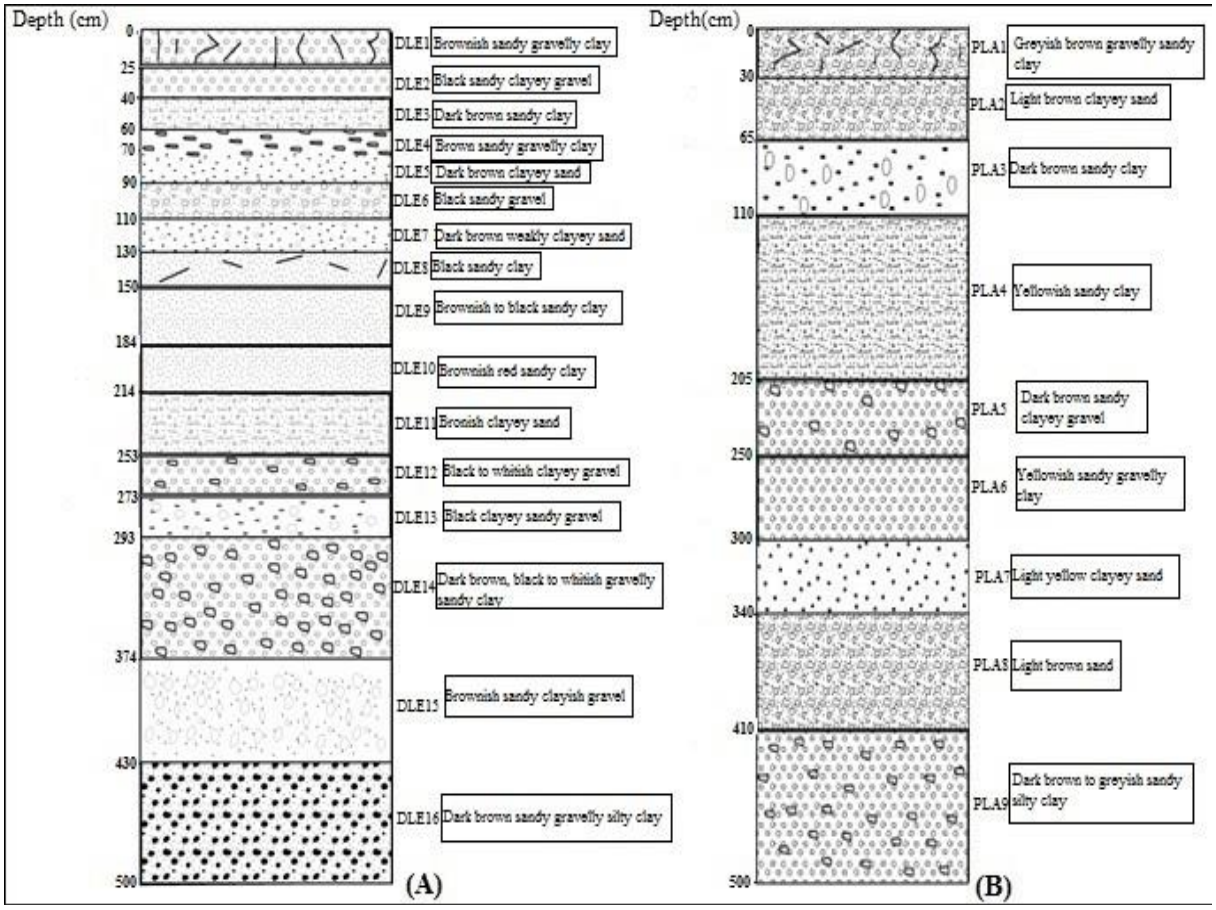

Fig. 4:Two profiles in Babouri-Figuil Quatenary deposits (A: pit in Délélé; B: pit in Pomla)

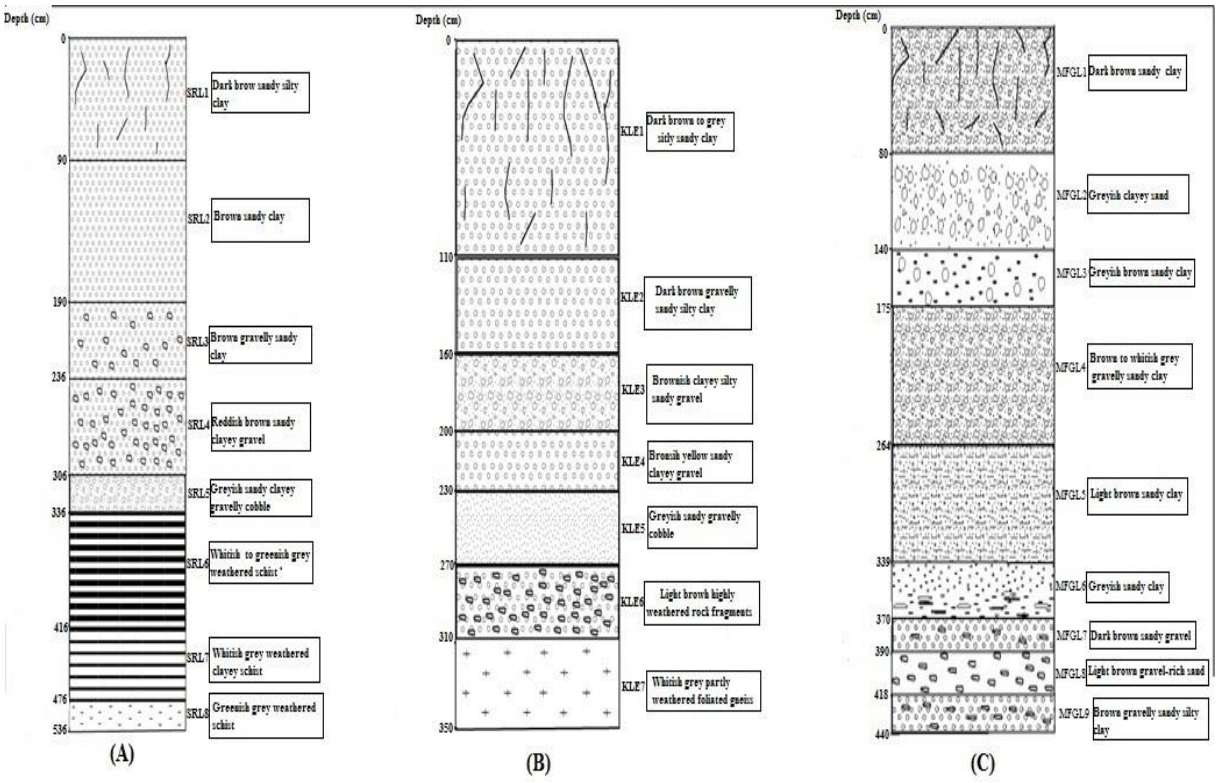

Fig. 5: Three profiles in Babouri-Figuil Quatenary deposits (A: pit in Sorawel; B: pit in Kolé; C: pit in Mayo Figuil).

V. Results

Trace and rare earth element compositions for mudrocks (mudstones and schistose marls) and unconsolidated fine-grained-rich Quaternary materials from pits are presented separately.

A. Mudrocks

Trace and rare earth element contents for sixten (16) mudrocks collected in six outcrops (in Dafang, Mayo Tafal, and Mayo Figuil) are highly heterogenous (Table 1).

a) Trace elements

Three samples from Dafang show trace element variations, with Ba (494-530 ppm), Sr (202-376 ppm), Zn (144-157 ppm), Zr (93-152 ppm), and V (92-123 ppm) being the highest quantified elements; followed by that of Rb (67-88 ppm), Cr (58-89 ppm), Ni (41-52 ppm), Cu (40-50 ppm), Y (15-40 ppm), Co (23-30 ppm), and Ga (19-26 ppm). The Th (8-30 ppm), Sc (11-19 ppm), Nb (14-16 ppm), and Pb (6-17 ppm) contents, and those of Hf, Cs, Ge, U, Ta, and W ranging from 0.7 to 5 ppm, are the lowest. Normalized patterns in Fig. 6a show different behavior with a positive Sr and negative Zr, Rb, and Hf anomalies for DFG1.

The trace element abundances in three mudstones from Mayo Tafal show the predominance of Ba (625-745 ppm), Zr (543-719 ppm), Sr (167-210 ppm), and Rb (106-114 ppm); followed by those of V (68-84 ppm), Zn (52-61 ppm), Cr (50-62 ppm), Y (35-38 ppm), Ni (24-39 ppm), Nb (25-31 ppm), Pb (22-23 ppm), Ga (20-24 ppm), and Th (19-20 ppm). The Cu (14-19 ppm), Hf (12-18 ppm), Sc (13-16 ppm), and Co (12-15 ppm) contents, with those of Cs, Ge, U, Ta, and W, ranging from 0.28 to 3.4 ppm. Their normalized patterns (Fig. 6b) show almost the same behavior with remarkable positive Zr and Hf and negative Sr and Ba anomalies.

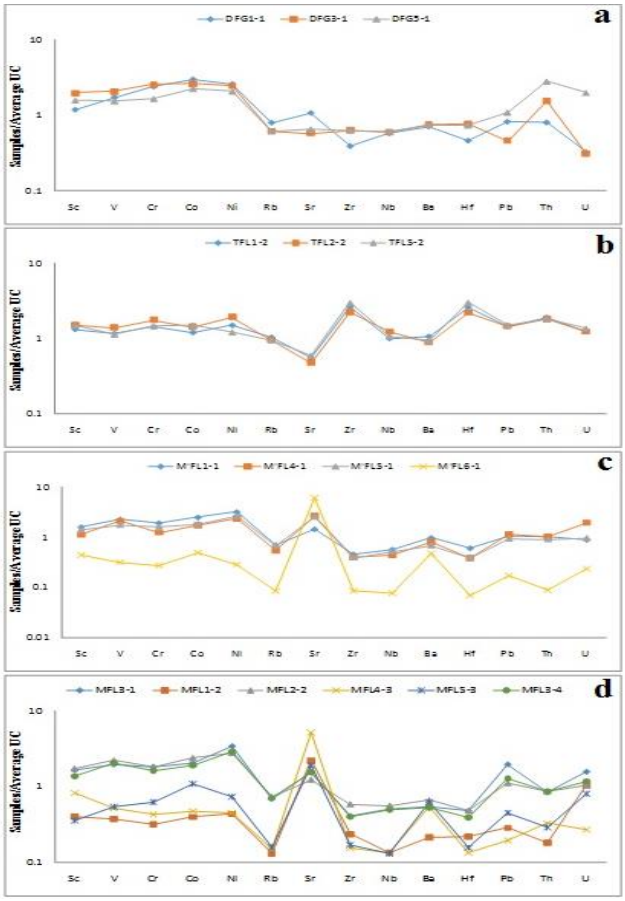

Fig. 6: Trace element patterns for the Babouri-Figuil mudrocks, normalized to Upper Crust values of [44] and plotted on Log10 versus trace element diagrams

Table 1 : Trace element concentration (in ppm) and calculated parameters for Babouri-Figuil mudrocks

Element and calculated parameters	Mayo Dafang			Mayo Tafal			Mayo Figuil									
	Mudstones			Mudstones			Schistose marls									
	DFG1-1	DFG3-1	DFG5-1	TFL1-2	TFL2-2	TFL5-2	M'FL1-1	M'FL4-1	M'FL5-1	M'FL6-1	MFL3-1	MFL1-2	MFL2-2	MFL4-3	MFL5-3	MFL3-4
Ba	494	530	517	745	625	671	684	560	481	336	375	151	465	378	437	378
Sr	376	202	227	195	167	210	509	916	896	2128	543	780	433	1816	664	538
Zr	93.0	152	150	631	543	719	109	94.0	94.0	21.0	98.0	57.0	141	37.0	41.0	96.0
Sc	11.9	19.7	15.7	13.2	15.3	14.9	16.0	11.1	14.1	4.4	16.6	4.0	17.3	8.2	36.0	13.8
V	104	123	92.0	70.0	84.0	68.0	138	125	104	19.1	117	23.0	133	31.0	33.0	124
Cr	84.0	89.0	58.0	50.0	62.0	52.0	67.0	43.0	56.0	9.6	64.0	11.1	63.0	15.0	22.0	57.0
Co	30.0	26.0	23.0	12.0	14.4	15.0	25.0	17.3	18.2	4.9	20.0	4.0	24.0	4.8	10.9	19.2
Ni	52.0	49.0	41.0	30.0	39.0	24.0	64.0	47.0	52.0	5.7	68.0	8.8	55.0	9.0	14.7	58.0
Cu	46.0	50.0	40.0	15.1	19.0	14.0	37.0	43.0	39.0	3.7	61.0	4.3	38.0	6.8	3.7	46.0
Zn	157	147	144	55.0	61.0	52.0	117	91.0	91.0	13.7	112	30.0	121	24.0	42.0	104
Ga	26.0	26.0	19.1	20.0	24.0	22.0	29.0	20.0	22.0	3.6	24.0	5.2	26.0	5.4	6.5	24.0
Rb	88.0	67.0	67.0	114	106	106	76.0	59.0	76.0	9.3	76.0	14.4	81.0	16.4	17.5	78.0
Y	15.2	33.0	40.0	38.0	37.0	35.0	36.0	41.0	26.0	10.4	34.0	11.4	29.0	23.0	17.1	27.0
Nb	14.4	14.9	15.2	25.0	31.0	27.0	14.1	11.0	12.9	1.9	12.5	3.4	14.1	3.4	3.3	12.5
Ge	1.37	3.1	1.46	1.52	1.68	1.76	2.9	4.1	1.97	0.22	1.96	0.83	3.3	0.58	0.76	2.4
Cs	3.1	2.2	2.1	2.5	3.1	2.8	2.9	2.4	2.5	0.48	2.5	0.93	2.9	0.74	0.75	2.6
Hf	2.7	4.5	4.2	15.0	12.9	17.5	3.5	2.2	2.3	0.41	2.8	1.27	2.8	0.78	0.90	2.3
Ta	0.89	0.95	0.95	1.69	2.0	2.1	0.94	0.76	0.87	0.07	0.88	0.21	0.96	0.16	0.6	0.83
W	1.96	3.2	2.8	0.83	0.76	0.72	2.1	0.99	1.45	< 0.05	3.1	0.72	3.3	0.89	1.03	1.94
Pb	12.6	6.9	16.3	22.0	22.0	23.0	15.8	17.1	14.0	2.6	30.0	4.3	16.8	2.9	6.7	19.3
Th	8.4	16.3	30.0	20.0	19.1	19.2	10.6	10.7	9.5	0.93	8.8	1.91	9.1	3.5	3.0	9.1
U	0.88	0.77	5.0	3.1	3.1	3.4	2.2	4.8	2.4	0.59	3.9	2.6	2.6	0.68	2.0	3.0
Zr/Hf	35.09	34.03	35.46	41.94	42.12	41.21	31.24	42.15	40.74	50.87	35.51	44.81	50.19	47.92	45.16	42.24
Y/Ni	0.29	0.67	0.98	1.27	0.95	1.46	0.56	0.87	0.50	1.82	0.50	1.30	0.53	2.56	1.16	0.47
Ni/Co	1.73	1.87	1.84	2.49	2.71	1.62	2.57	2.73	2.88	1.17	3.36	2.19	2.32	1.88	1.35	3.04
Cr/Ni	1.62	1.82	1.41	1.67	1.59	2.17	1.03	0.91	0.69	1.68	0.94	1.26	1.15	1.67	1.50	0.98
V/Cr	1.23	1.39	1.59	1.40	1.35	1.32	2.04	2.91	1.85	1.99	1.84	2.03	2.10	2.06	1.50	2.19
Th/Cr	0.1	0.18	0.51	0.4	0.31	0.37	0.16	0.25	0.17	0.10	0.14	0.17	0.14	0.23	0.14	0.16
Cr/Th	10.0	5.46	1.93	2.5	3.26	2.70	6.32	4.02	5.89	10.32	7.27	5.81	6.92	4.29	7.33	6.26
Th/Co	0.28	0.62	1.31	1.66	1.33	1.28	0.42	0.62	0.52	0.19	0.43	0.48	0.38	0.73	0.28	0.48
U/Th	0.10	0.05	0.17	0.15	0.16	0.18	0.21	0.45	0.25	0.63	0.44	1.36	0.29	0.19	0.67	0.33
Th/Sc	0.71	0.83	1.88	1.51	1.25	1.29	0.66	0.96	0.67	0.21	0.53	0.48	0.53	0.42	0.85	0.66
Ga/Rb	0.30	0.39	0.29	0.18	0.23	0.21	0.38	0.34	0.29	0.39	0.32	0.36	0.32	0.33	0.37	0.31
Sr/Cu	8.17	4.04	5.68	12.91	8.79	15	13.76	21.30	22.97	575.14	8.90	181.40	11.39	267.06	179.46	11.70
Sr/Ba	0.76	0.38	0.44	0.26	0.27	0.31	0.74	1.64	1.86	6.33	1.45	5.17	0.93	4.80	1.52	1.42
V/Ni	1.99	2.52	2.22	2.33	2.16	2.79	2.15	2.65	1.99	3.33	1.72	2.61	2.41	3.44	2.21	2.13
V/V+Ni	0.67	0.72	0.69	0.70	0.68	0.74	0.68	0.73	0.67	0.77	0.63	0.72	0.71	0.77	0.69	0.68
δU=2U(U+Th/3)	0.48	0.24	0.67	0.63	0.65	0.69	0.77	1.15	0.86	1.31	1.14	1.60	0.92	0.74	1.33	0.99
AU=U-Th/3	-4.55	-4.66	-5.0	-3.57	-3.27	-3.0	-1.33	1.23	-0.77	0.28	0.96	1.96	-0.43	-0.49	1.0	-0.03

Ten samples of schistose marls from four outcrops at Mayo Figuil show compositional differences. They are predominantly composed of Sr (433-2128 ppm) and Ba (336-684 ppm). The V (19-138 ppm), Zn (13-121 ppm), Zr (21-141 ppm), Rb (9.0-84 ppm), Ni (5.0-68 ppm), Cu (3-61 ppm), Ga (3-29 ppm), and Co (4-25 ppm) are significant. The Pb (2-18 ppm), Sc (4-16 ppm), and Th (0.9-11 ppm) contents and those of Cs, Ge, U, Ta, and W ranging from < 0.05 to 5.0 ppm, are the lowest. The highest Rb content is found in M'FL6-1 and MFL4-3, which generally encloses the lowest content of other quantified trace elements. The normalized plots in Figs. 6b-c distinguish two main groups with (1) those with strong to slightly weak positive Zr, Ba, Pb, and U anomalies; and (2) those with weak to very weak positive anomalies of those elements.

b) Rare earth elements

The REE concentrations in Table 2 for all mudrocks show variation with the predominance of light rare earth elements (LREE : La-Eu) over heavy rare eath elements (HREE: Gd-Lu). Mudstones from Dafang show total LREE (∑LREE) and HREE (∑HREE) concentrations (in ppm) ranging from 123 to 140, and 11 to 25, respectively. The LREE/ HREE ratios and total rare earth elements (∑REE) concentrations range from 5.0 to 11.0 and 135 to 163 ppm, respectively. The calculated $(Ce/Ce^*)_N$, $(La/La^*)_N$, and $(Pr/Pr^*)_N$ values range from 1.08 to 1.11 (no anomaly), 0.87 to 0.96 (a slightly negative anomaly), and 0.99 to 1.02 (no anomaly), respectively, are visible in the normalized patterns plots (Fig. 7a). Fig.7a shows overlaping of DFG3-1 and DFG5-1 plots separate to that of DFG1-1.

The LREE and HREE concentrations in mudstones from Mayo Tafal range from 198 to 206 ppm and 20 to 22 ppm, respectively. The LREE/HREE ratios and ∑REE contents range from 9.1 to 9.8, and 220-235 ppm. The calculated $(Ce/Ce^*)_N$, $(La/La^*)_N$, and $(Pr/Pr^*)_N$ values range from 0.89 to 1.0 (a slightly negative to no anomaly), 0.84 to 1.03 (a slightly negative no anomaly), and 0.97 to 1.05 (a slightly negative to weakly positive anomaly), respectively. The plotted normalized patterns (Fig. 7b) show almost the same behavior, although Ce and Er anomalies show some differences.

The LREE and HREE concentrations in schistose marls from Mayo Figuil range from 28 to 191 ppm and 5.0 to 24 ppm, respectively. Two groups are distinguished within schistose marls : those with relatively high LREE and HREE contents (e.g., M'FL4-1 and MFL3-1) and those with relatively low values (e.g., M'FL6-1 and MFL5-3). The LREE/HREE ratios and ∑REE concentrations range from 5.0 to 10 and 33 to 215 ppm, respectively. The calculated $(Ce/Ce^*)_N$, $(La/La^*)_N$, and $(Pr/Pr^*)_N$ range from 0.78 to 1.04 (negative to no anomaly), 0.84 to 1.38 (negative to positive anomaly), 1.06 to 1.10 (slight positive anomaly) in schistose marls. The normalized patterns for schistose marls with some overlap (Figs. 7c-d), distinguish those with almost flat plots and those with positive Yb anomaly.

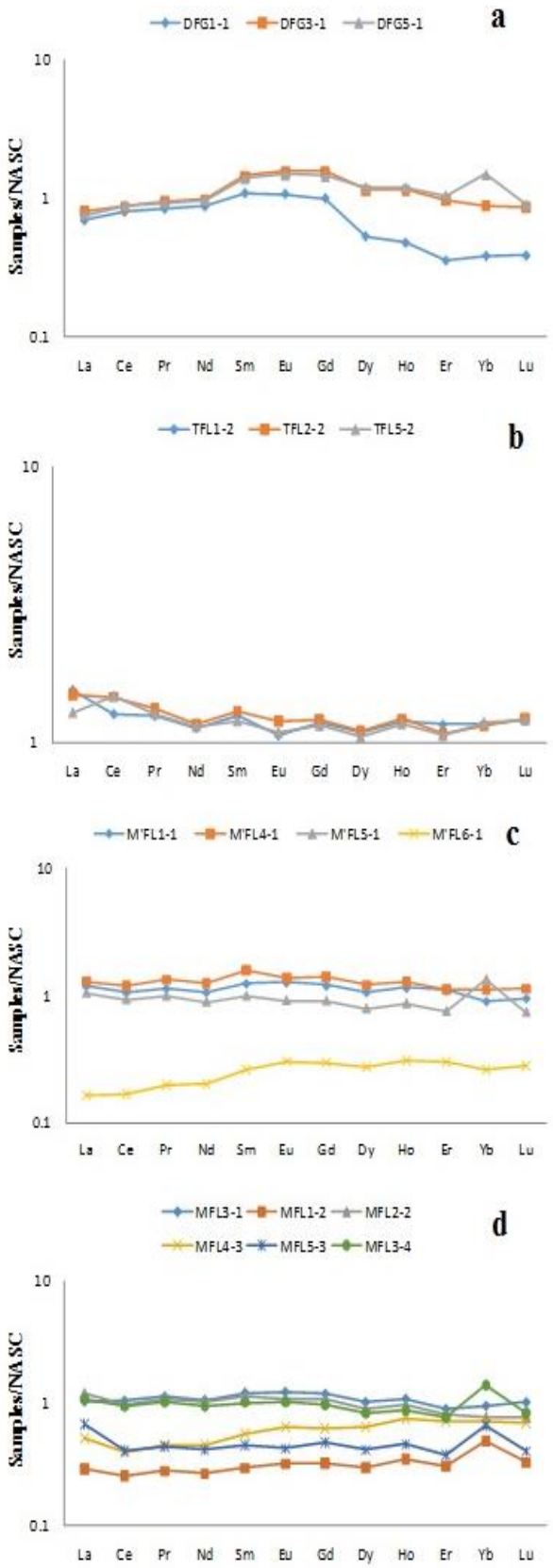

Fig. 7: REE patterns for the Babouri-Figuil mudrocks, normalized to North American shale composite values of [45] and plotted on Log10 versus element (La–Lu) diagrams (a: Dafang mudstones; b: Mayo Tafal mudstones; c-d: Mayo Figuil schistose marls).

Table 2 : Rare earth element concentration (in ppm) and calculated parameters for Babouri-Figuil mudrocks

Element and calculated parameters	Mayo Dafang			Mayo Tafal			Mayo Figuil									
	Mudstones			Mudstones			Schistose marl									
	DFG1-1	DFG3-1	DFG5-1	TFL1-2	TFL2-2	TFL5-2	M'FL1-1	M'FL4-1	M'FL5-1	M'FL6-1	MFL3-1	MFL1-2	MFL2-2	MFL4-3	MFL5-3	MFL3-4
La	22.0	26.0	24.0	50.0	48.0	41.0	38.0	42.0	34.0	5.3	33.0	9.3	36.0	16.0	22.0	34.0
Ce	58.0	63.0	65.0	93.0	107	108	77.0	87.0	68.0	12.5	76.0	18.4	71.0	29.0	30.0	69.0
Pr	6.7	7.5	7.3	9.9	10.5	10.1	9.0	10.5	7.9	1.6	8.8	2.2	8.6	3.6	3.5	8.1
Nd	29.0	33.0	32.0	37.0	39.0	38.0	35.0	41.0	29.0	6.8	35.0	8.7	34.0	15.1	13.7	31.0
Sm	6.2	8.3	7.9	7.1	7.4	6.8	7.1	9.1	5.7	1.50	6.8	1.2	6.5	3.2	2.6	5.7
Eu	1.34	1.94	1.84	1.32	1.48	1.36	1.58	1.71	1.14	0.38	1.51	0.39	1.33	0.79	0.53	1.25
Gd	5.2	8.1	7.5	6.2	6.3	6.0	6.3	7.4	4.7	1.56	6.1	1.68	5.6	3.2	2.5	5.0
Dy	3.0	6.4	6.7	6.0	6.1	5.8	5.9	6.7	4.4	1.54	5.6	1.65	4.9	3.6	2.3	4.6
Ho	0.50	1.20	1.25	1.25	1.27	1.22	1.20	1.32	0.90	0.32	1.12	0.36	1.0	0.78	0.48	0.90
Er	1.22	3.3	3.6	4.0	3.7	3.7	3.7	3.8	2.6	1.03	3.0	1.04	2.7	2.4	1.28	2.6
Yb	1.20	2.7	4.6	3.7	3.6	3.6	2.8	3.5	4.2	0.82	2.9	1.53	2.3	2.2	2.0	4.3
Lu	0.19	0.41	0.43	0.58	0.59	0.58	0.46	0.54	0.36	0.14	0.48	0.16	0.37	0.33	0.20	0.40
LREE	123.82	139.09	138.52	198.67	212.72	205.44	168.06	190.97	145.80	28.13	160.23	40.63	159.83	68.01	71.79	148.91
HREE	11.29	22.11	24.11	21.65	21.47	20.96	20.35	23.22	17.12	5.40	19.23	6.42	16.97	12.55	8.80	17.86
LREE/ HREE	10.97	6.29	5.75	9.18	9.91	9.80	8.26	8.22	8.52	5.21	8.33	6.33	9.42	5.42	8.16	8.34
∑REE	135.10	161.20	162.63	220.32	234.19	226.40	188.42	214.19	162.92	33.53	179.46	47.05	176.80	80.55	80.59	166.77
La/Sm	3.57	3.07	3.06	6.97	6.43	6.02	5.34	4.58	5.93	3.55	4.78	5.57	5.90	5.23	8.44	5.97
Gd/Yb	4.35	2.97	1.63	1.69	1.76	1.64	2.23	2.12	1.14	1.89	2.10	1.10	2.34	1.46	1.22	1.16
La/Yb	18.53	9.67	5.24	13.65	13.40	11.21	13.60	11.98	8.09	6.48	11.23	6.07	16.15	7.48	10.63	7.86
La/Co	0.73	1.0	1.04	4.17	3.33	2.73	1.52	2.43	1.87	1.08	1.65	2.33	1.50	3.33	2.02	1.77
La/Sc	1.87	1.30	1.55	3.76	3.12	2.76	2.39	3.74	2.38	1.21	1.98	2.32	2.23	2.02	6.11	2.47
Y/Ho	44.43	21.31	19.47	39.76	37.75	33.75	31.75	31.03	37.76	16.47	29.30	25.84	38.63	21.15	45.33	37.93
$(Gd/Yb)_N$	2.58	1.79	0.97	1.00	1.04	1.00	1.34	1.26	0.67	1.13	1.25	0.65	1.45	0.87	0.75	0.69
Dy_N/Sm_N	0.50	0.799	0.87	0.87	0.85	0.88	0.85	0.76	0.79	1.06	0.85	1.41	0.78	1.16	0.91	0.83
La_N/Yb_N	1.78	0.93	0.51	1.31	1.29	1.10	1.31	1.16	0.78	0.63	1.10	0.59	1.52	0.71	1.07	0.77
Gd_N/Yb_N	2.58	1.79	0.97	1.00	1.04	0.99	1.34	1.26	0.67	1.13	1.25	0.65	1.45	0.87	0.75	0.69
$(La/La^*)_N$	0.87	0.96	0.91	1.03	0.92	0.84	0.92	0.87	0.86	0.85	0.84	0.94	0.93	1.11	1.38	0.89
$(Pr/Pr^*)_N$	1.01	1.02	0.99	1.05	1.00	0.97	1.08	1.09	1.10	1.07	1.06	1.08	1.09	1.07	1.07	1.09
$(Ce/Ce^*)_N$	1.11	1.08	1.10	0.89	0.94	1.00	0.98	1.01	0.97	1.10	1.04	0.98	0.98	0.95	0.78	0.98
δCe	0.68	0.56	0.64	0.33	0.37	0.45	0.39	0.34	0.44	2.55	0.45	1.56	0.40	0.87	0.67	0.43

B. Quaternary deposits

Trace and rare earth element contents for twenty five (25) samples (Tables 3 and 4) collected in five pits dug in unconsolidated Quarternary deposits (in Délélé: DLE, Pomla: PLA, Sorawel: SRL, Kolé: KLE, and Figuil : MFGL) are presented. These elements concentrations are heterogneous and mainly different from one level to another and from one pit to another.

a)Trace elements

Trace element concentrations in seven samples from Délélé (DLE) (Table 3) show the predominance of Sr (289-416 ppm) and Ba (326-652 ppm) with the highest Sr values found in DLE3, DLE10, and DLE16, which also enclose the lowest Ba contents. The Zr and V contents range from 113 to 203 ppm and 97 to 141 ppm, respectively. The contents of Sc, Cr, Co, Cu, Ni, Zn, Ga, Y, and Rb range from 7.0 to 80 ppm with the highest values (> 40 ppm) being those of Cr and Zn. Those of Nb, Ge, Cs, Hf, Ta, U, Th, W, and Pb vary from 0.3 to 8.7 ppm with the highest values (> 6.0 ppm) being those of Nb and Pb. The plotted normalized patterns in Fig. 8a show a distinctive feature (mainly for Ba anomaly) with some samples showing weakly positive anomalies and others, with no anomalies.

Five samples (PLA) from Pomla have relatively high Ba, Zr, and Sr contents, ranging from 456 to 766 ppm, 298 to 874 ppm, and 203 to 324 ppm, respectively. Samples with the highest Ba contents also have the highest Zr contents. The Y, Ni, Co, Th, Sc, Pb, Hf, Nb, Ga, Cu, Cr, Zn and Rb contents range from 7.0 to 110 ppm with the highest values (> 40 ppm) being those of Y, Zn, Cr, V, and Rb. The Ge, Cs, Ta, W, and U contents vary from 0.8 to 4.0 ppm. The normalized patterns in Fig. 8b show four distinctive features, including that of Ni, Rb, Sr, Zr, Ba, Hf, Pb, and Th, which show positive, weakly negative, or no anomalies.

The trace element contents and their normalized patterns in Fig 8c for samples from Sorawel (SRL), show extreme variations and differences. Within these element's suites, Ba (181-1065 ppm), Zr (105-521 ppm), and Sr (448-666 ppm) contents are the highest. The lowest Zr value is found in SRL8, which encompass the highest Sr content. The highest Ba content is found in SRL1, which include the lowest Sr content. The Cr, Ni, V, Cu, Y, Zn, and Rb contents generally range from 30 to 293 ppm with the highest values being those of V, Cr, Ni, Zn, and/or Cu mainly found in SRL7 and SRL8. The Sc, Co, Ga, Nb, Hf, Th, and Pb concentrations dominantly range from 6 to 47 ppm with the highest values being those of Zn, Pb, Ga, and Y found in SRL4, SRL7, and/or SRL8. The Ge, Cs, Ta, W, and U contents range from < 0.05 to 7.0 ppm. The normalized plots (Fig. 8c) show no major correlation. Some plots, notably that of SRL2, SRL3, and SRL4, show a strong positive Zr anomaly.

The trace element contents in two samples from Kolé (KLE1 and KLE4) and plotted normalized patterns (Fig. 8d) show clear differences with Ba (≤ 598 ppm), Sr (≤ 460 ppm), and Zr (≤ 269 ppm). The Ga, Zn, Sc, V, Cr, Co, Ni, Rb, Y, and Nb contents range from 5 to 75.0 ppm with the highest values being those of V, Zn, and Rb found in KLE1. The Cu, Cs, Hf, Ta, W Pb, Th, and W contents vary from < 0.05 to 10 ppm with the highest values being those Cu and Pb. The plotted patterns in Fig. 8d show positive anomalies for Co, Sr, Zr, and Ba for KLE4-1 and no anomaly of these element in KLE2-1.

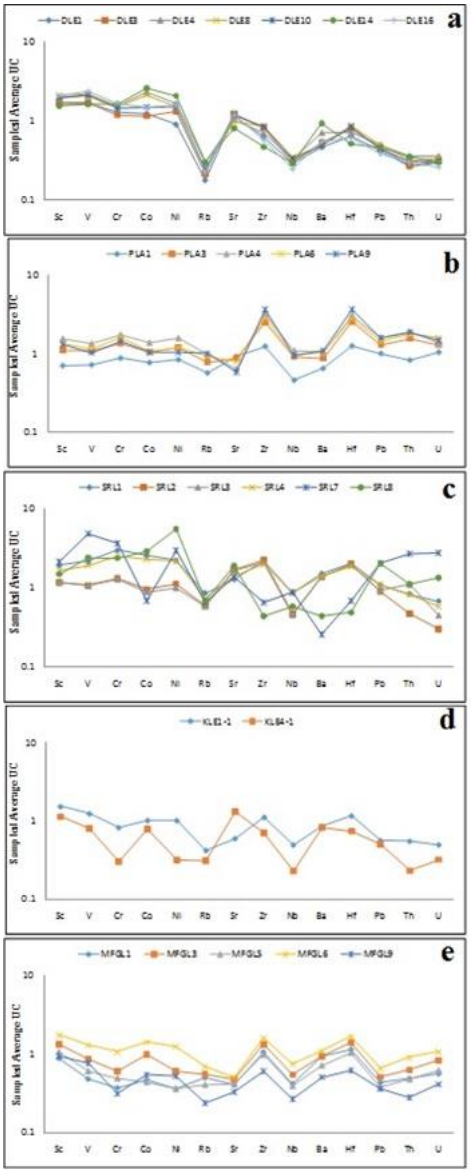

Fig. 8 Trace element patterns for the Babouri-Figuil fine-grained-rich Quaternary deposits, normalized to Upper Crust values of [44] and plotted on Log10 versus trace element diagrams (a: samples from Délélé; b: samples from Pomla; c: samples from Sorawel; d: samples from Kolé; e: samples from Mayo Figuil).

Table 3 : Trace element concentration (in ppm) and calculated parameters of the Babouri-Figuil fine-grained-rich Quatenary deposits.

Element and calculated parameters	Délélé							Pomla					Sorawel						Kolé		Figuil				
	Mayo Délélé							Mayo Louti					Mayo Sorawel						Mayo Kolé		Mayo Figuil				
	DLE1	**DLE3**	**DLE4**	**DLE8**	**DLE10**	**DLE14**	**DLE16**	**PLA1**	**PLA3**	**PLA4**	**PLA6**	**PLA9**	**SRL1**	**SRL2**	**SRL3**	**SRL4**	**SRL7**	**SRL8**	**KLE1**	**KLE4**	**MFGL 1**	**MFGL 3**	**MFGL 5**	**MFGL 6**	**MFGL 9**
Ba	326	363	493	336	344	652	379	456	607	737	734	766	1065	961	978	993	181	305	598	577	656	661	509	774	361
Sr	406	427	359	345	411	283	416	324	303	225	275	203	448	594	583	496	489	666	210	460	145	169	147	176	117
Zr	151	195	167	204	203	113	138	298	602	760	701	874	521	537	505	481	158	105	269	168	254	325	238	390	148
V	101	102	128	131	127	97.0	141	44.0	66.0	81.0	68.0	62.0	130	64.0	64.0	116	293	146	75.0	40.0	29.0	52.0	37.0	78.0	46.0
Cr	45.0	41.0	54.0	52.0	51.0	58.0	59.0	31.0	48.0	61.0	57.0	51.0	105	45.0	45.0	89.0	128	83.0	29.0	10.6	13.1	21.0	17.5	38.0	11.1
Co	12.3	23.0	21.0	15.0	26.0	14.7	7.7	10.5	13.9	10.7	10.4	26.0	9.6	9.0	9.0	23.0	6.9	29.0	10.2	7.8	4.7	9.9	4.5	14.4	5.5
Ni	18.1	26.0	33.0	30.0	31.0	42.0	32.0	16.8	24.0	32.0	24.0	21.0	44.0	22.0	20.0	44.0	59.0	112	20.0	6.3	7.3	12.2	7.3	25.0	10.6
Cu	15.5	27.0	39.0	35.0	34.0	33.0	36.0	14.3	13.5	18.0	18.3	17.2	41.0	2.9	< 0.5	25.0	176	123	9.6	< 0.5	4.5	3.9	3.7	20.0	11.5
Zn	38.0	42.0	65.0	58.0	56.0	79.0	49.0	27.0	44.0	55.0	44.0	39.0	87.0	33.0	31.0	75.0	51.0	137	61.0	47.0	35.0	40.0	27.0	62.0	26.0
Ga	15.8	17.0	21.0	17.5	19.2	16.8	16.1	12.9	18.1	22.0	19.8	19.4	26.0	17.1	17.7	25.0	34.0	21.0	19.6	16.8	13.8	17.8	14.6	23.0	11.0
Rb	19.5	23.0	33.0	26.0	27.0	33.0	25.0	63.0	86.0	102	106	110	94.0	65.0	65.0	81.0	72	75.0	47.0	34.0	56.0	61.0	45.0	76.0	27.0
Y	18.3	17.9	22.0	26.0	24.0	36.0	21.0	79.0	46.0	33.0	44.0	42.0	46.0	20.0	20.0	39.0	47.0	34.0	42.0	19.3	31.0	47.0	33.0	64.0	23.0
Sc	16.5	16.9	19.5	21.0	19.9	15.5	21.0	7.1	11.0	15.6	13.3	13.2	19.3	11.7	11.8	16.5	22.0	14.9	15.3	5.7	10.6	13.8	10.0	18.9	9.6
Nb	7.3	7.3	8.2	8.7	8.2	7.3	6.1	11.6	23.0	28.0	24.0	24.0	22.0	11.8	11.4	21.0	22.0	15.6	12.4	11.3	1.45	13.4	10.7	17.7	1.48
Ge	1.36	1.35	1.40	1.47	1.68	1.24	1.40	1.04	1.40	1.71	2.6	1.51	1.69	1.13	1.16	1.60	3.4	2.10	1.59	1.12	8.9	2.0	1.82	1.86	6.8
Cs	0.59	0.88	1.24	0.96	0.94	1.29	1.01	1.46	2.2	2.7	16.4	2.3	2.1	0.83	0.85	1.93	3.7	2.6	1.31	0.95	0.76	1.02	0.74	1.54	0.5
Hf	3.8	4.6	4.1	4.9	4.9	3.0	3.5	7.3	14.9	17.7	1.67	21.0	12.0	11.5	11.5	10.9	4.0	2.8	6.8	4.3	6.6	8.2	6.1	9.7	3.7
Ta	0.5	0.48	0.53	0.59	0.53	0.45	0.45	0.80	1.65	1.90	1.64	1.68	1.22	0.70	0.65	1.18	1.48	0.95	0.79	0.25	0.89	1.11	0.80	1.44	0.55
W	0.73	0.38	0.30	0.33	0.48	0.62	0.62	0.85	1.11	2.5	1.65	1.97	1.87	< 0.05	< 0.05	0.48	5.6	2.5	0.29	< 0.05	< 0.05	0.63	0.45	0.95	0.65
Pb	6.3	6.90	7.50	7.4	6.7	6.9	5.7	15.1	19.5	24.0	22.0	24.0	16.3	13.5	14.1	16.2	31.0	31.0	8.5	7.5	6.6	7.7	5.8	9.9	5.5
Th	2.8	2.8	3.8	3.3	3.3	3.7	3.1	8.7	16.3	20.0	18.8	19.7	8.8	5.5	11.8	8.6	28.0	11.6	5.8	2.4	5.2	6.6	5.1	9.6	3.0
U	0.74	0.77	0.90	0.84	0.77	0.77	0.65	2.6	3.2	3.4	4.0	3.7	1.69	0.75	1.13	1.44	6.9	3.4	1.25	0.8	1.42	2.1	1.58	2.7	1.05
Ba/Sc	19.76	21.48	25.28	16.0	17.29	42.06	18.04	64.23	55.18	47.24	55.19	58.03	55.18	82.14	82.88	60.18	8.23	20.47	39.08	101.23	61.89	47.90	50.9	40.95	37.60
Y/Ni	1.01	0.69	0.67	0.87	0.77	0.86	0.66	4.70	1.92	1.03	1.83	2.0	1.05	0.91	1.0	0.89	0.80	0.30	2.1	3.06	4.25	3.85	4.52	2.56	2.17
Ba/Co	26.50	15.78	23.48	22.4	13.23	44.35	49.22	43.43	43.67	70.89	70.58	29.46	110.94	106.78	108.67	43.17	26.23	10.52	58.63	73.97	139.57	66.77	113.11	53.75	65.64
Zr/Hf	40.20	42.31	40.58	41.25	41.28	37.83	39.00	40.81	40.44	42.84	42.65	41.18	43.57	46.73	44.09	44.20	39.23	37.37	39.75	39.22	38.51	39.57	39.18	40.34	40.22
Ni/Co	1.47	2.26	1.43	1.43	2.04	1.60	2.16	2.18	2.30	2.28	2.59	2.00	1.73	2.35	2.25	1.89	8.65	3.83	1.99	0.81	1.54	1.24	1.64	1.74	1.90
V/Cr	2.23	2.49	2.36	2.51	2.46	1.69	2.41	1.41	1.38	1.33	1.19	1.21	1.23	1.42	1.42	1.30	2.29	1.76	2.58	4.59	2.22	2.40	2.11	2.07	4.18
Th/Cr	0.06	0.07	0.07	0.06	0.07	0.06	0.05	0.28	0.34	0.33	0.33	0.39	0.08	0.11	0.26	0.10	0.22	0.14	0.20	0.23	0.40	0.31	0.29	0.25	0.27
Cr/Th	16.08	14.64	14.21	13.68	13.42	15.68	19.31	8.38	2.94	3.05	3.03	2.59	27.63	8.18	3.81	10.83	4.57	7.16	5.0	4.42	2.52	3.18	3.43	3.96	3.70
Th/Co	0.23	0.24	0.17	0.16	0.22	0.14	0.21	1.13	1.56	1.44	1.75	1.90	0.34	0.51	1.31	0.37	4.14	0.4	0.57	0.31	1.11	0.67	1.14	0.67	0.54
U/Th	0.26	0.28	0.24	0.25	0.23	0.21	0.21	0.30	0.20	0.17	0.21	0.19	0.22	0.14	0.10	0.40	0.25	0.29	0.22	0.33	0.27	0.32	0.31	0.28	0.35
Th/Sc	0.17	0.17	0.20	0.16	0.16	0.24	0.15	1.23	1.47	1.28	1.41	1.50	0.46	0.42	0.99	0.52	1.31	0.78	0.38	0.22	0.58	0.49	0.47	0.54	0.31
Ga/Rb	0.81	0.73	0.65	0.66	0.72	0.51	0.65	0.20	0.21	0.21	0.19	0.18	0.28	0.26	0.27	0.31	0.47	0.29	0.42	0.49	0.25	0.29	0.32	0.30	0.41
Sr/Cu	26.19	15.77	9.26	9.85	12.02	8.51	11.61	22.71	22.48	12.54	15.07	11.75	10.98	205.91	< 1166	19.73	2.79	5.41	21.90	< 920	31.89	42.85	40.01	8.70	10.11
V/V+Ni	0.85	0.80	0.80	0.81	0.81	0.70	0.82	0.73	0.73	0.72	0.74	0.75	0.74	0.74	0.75	0.73	0.83	0.57	0.79	0.88	0.80	0.81	0.84	0.76	0.81
δU	0.89	0.91	0.83	0.87	0.82	0.77	0.77	0.95	0.74	0.68	0.79	0.72	0.73	0.58	0.45	0.67	0.85	0.94	0.77	1.0	0.90	0.49	0.96	0.92	1.02

Quantified elements in five samples from Mayo Figuil (MFGL) show relatively high Zr (148-390 ppm), Sr (145-176 ppm), and Ba (361-774 ppm). The highest Ba and Zr concentrations are found in MFGL6 and MFGL9. The Rb, V, Zn, and Y range from 23 to 78 ppm with the highest values being generally those of Rb and V. The Sc, Cr, Ni, Ga, and Nb range from 6 to 25 ppm. The concentration of Co, Cu, Ge, Cs, Hf, Ta, W, Th, U, and Pb varies from < 0.05 to 20 ppm with the highest values being those of Co, Cu, and Hf. The normalized plotted data in Fig. 8e, generally show correlations, except those of MFGL9, which shows a difference in from Sc to Rb and from Pb to U.

b) Rare earth elements

The total LREE and HREE contents in samples from Délélé vary from 68 to 131 ppm and 10 to 20 ppm, respectively. The LREE/ HREE ratios and total rare earth elements (∑REE) concentrations range from 5.0 to 7.0 and 79 to 150 ppm. The lowest ∑REE concentration is that of DLE1, and the highest in DLE14. Those in DLE3, DLE4, DLE8, and DLE10 and DLE16 with some similarities, range from 90 to 103 ppm. The normalized plots in Fig. 9a show almost the same behavior, excepting that of DLE14 with a negative Ce and positive Yb anomaly.

The total LREE, HREE, and REE concentrations in samples from Pomla range from 187 to 282 ppm, 20 to 36 ppm, and 211 to 318 with the highest value found in PLA1 and PLA3. The LREE/ HREE ratios vary from 7.0 to 11.0 with the highest value being that of PLA4. Plotted normalized REE values in Fig. 9b show distinctive behaviors with a: strong negative Ce anomaly and no Eu anomaly for PLA1; weak positive Ce anomaly and strong positive Yb anomaly for PLA2; and weak negative Ce and Ho anomaly for PLA3.

The ∑LREE, ∑HREE, and ∑REE for samples from Sorawel range from 114 to 278 ppm, 14 to 29 ppm, and 128 to 304 ppm with the highest values found in SRL1 and SRL7. The LREE/ HREE ratios range from 8 to 15 with the highest value found in SRL3. The plotted normalized data in Fig. 9c show almost the same behavior (generally increasing from La to Eu and decreasing from Eu to Lu); excepting those of SRL2 and SRL3. SRL2 plot is characterized with a positive Eu and Yb anomaly; and SRL3 show much flatter plot with no Eu anomaly.

The total LREE and HREE contents in samples from Kolé is up to 127.58 ppm and 23.43 ppm, respectively. The LREE/HREE ratios and ∑REE vary from up to 7.33 and up to 151 ppm, respectively. Plotted normalized values in Fig. 9d show distinctive feature: that of KLE1-1 increases slowly from La to Lu; and KLE4-1, increases from La to Eu, and decreases from Eu to Lu.

The ∑LREE, ∑HREE, and ∑REE for samples from Mayo Figuil range 78 to 182 ppm, 13 to 35 ppm, and 92 to 217 ppm, respectively. The LREE/ HREE ratios range from 4.0 to 6.0. The normalized patterns plots in Fig. 9e show almost the same behavior increasing slowly from Ce to Lu. The main difference is the Ce anomaly (weak positive anomaly for MFGL3 and weak negative anomaly for MFGL6).

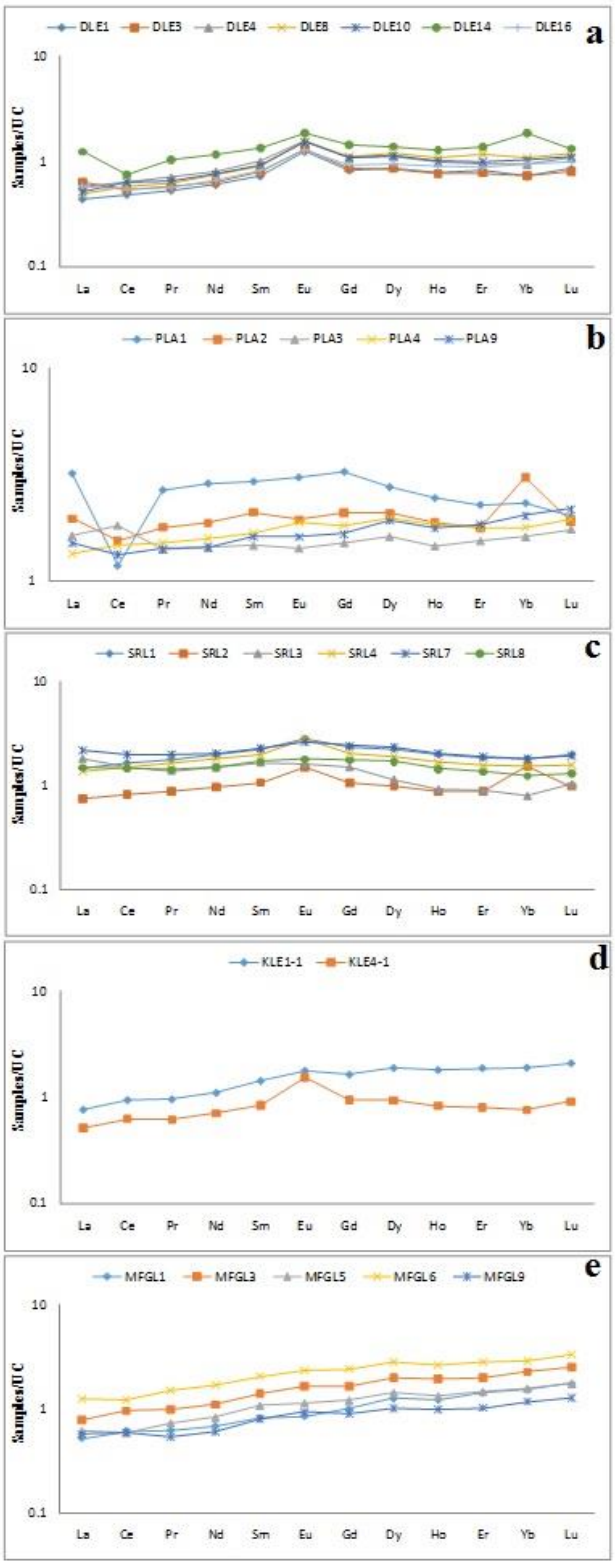

Fig. 9 : REE patterns for the Babouri-Figuil fine-grained-rich Quaternary deposits, normalized to North American shale composite values of [45] and plotted on Log10 versus element (La–Lu) diagrams(a: samples from Délélé; b: samples from Pomla; c: samples Sorawel; d: samples from Kolé; e: samples from Mayo Figuil).

Table 4 : Rare earth element concentration (in ppm) and calculated parameters of the Babouri-Figuil fine-grained-rich Quatenary deposits

Element and calculated parameters	Délélé							Pomla					Sorawel					Kolé			Figuil				
	Mayo Délélé							Mayo Louti					Mayo Sorawel					Mayo Kolé			Mayo Figuil				
	DLE1	DLE3	DLE4	DLE8	DLE10	DLE14	DLE16	PLA1	PLA3	PLA4	PLA6	PLA9	SRL1	SRL2	SRL3	SRL4	SRL7	SRL8	KLE1	KLE4	MFGL1	MFGL3	MFGL5	MFGL6	MFGL9
La	13.3	19.3	17.3	14.9	15.4	37.0	17.7	96.0	59.0	49.0	40.0	45.0	44.0	23.0	55.0	41.0	67.0	45.0	23.0	15.4	15.7	23.0	18.5	38.0	17.3
Ce	31.0	35.0	40.0	37.0	41.0	48.0	35.0	76.0	100	117	94.0	85.0	107	54.0	98.0	96.0	128	95.0	61.0	40.0	40.0	61.0	38.0	78.0	38.0
Pr	3.8	4.1	5.0	4.4	4.6	7.3	4.1	19.0	12.8	10.0	10.8	10.1	12.7	6.3	9.9	11.8	14.5	10.2	6.9	4.4	4.4	7.0	5.2	10.7	3.8
Nd	15.8	16.7	21.0	19.5	19.8	30.0	17.3	75.0	49.0	37.0	41.0	38.0	52.0	25.0	39.0	47.0	53.0	39.0	29.0	18.7	17.9	29.0	22.0	44.0	15.7
Sm	3.3	3.6	4.5	4.1	4.2	6.0	3.8	13.2	9.5	6.6	7.6	7.3	10.1	4.9	7.5	8.9	10.4	7.8	6.4	3.8	3.7	6.4	4.9	9.2	3.6
Eu	1.09	1.17	1.38	1.37	1.35	1.65	1.14	2.7	1.71	1.26	1.66	1.43	2.5	1.34	1.43	2.5	2.3	1.59	1.57	1.37	0.75	1.46	1.01	2.1	0.83
Gd	3.2	3.3	4.1	4.3	4.1	5.5	3.6	12.4	7.9	5.8	7.0	6.4	8.9	4.1	5.7	7.7	9.3	6.8	6.2	3.6	3.8	6.4	4.6	9.2	3.4
Dy	3.0	3.0	3.9	4.2	4.0	4.9	3.4	9.7	7.3	5.7	7.0	6.8	7.9	3.5	4.0	6.6	8.3	6.0	6.6	3.3	4.4	7.0	5.1	9.8	3.6
Ho	0.63	0.62	0.79	0.87	0.80	1.03	0.73	1.97	1.51	1.17	1.48	1.43	1.59	0.71	0.74	1.34	1.67	1.16	1.44	0.67	0.99	1.56	1.08	2.2	0.80
Er	1.91	1.72	2.2	2.7	2.2	3.2	2.0	5.3	4.1	3.6	4.1	4.3	4.3	2.1	2.0	3.6	4.4	3.1	4.3	1.85	3.3	4.6	3.4	6.5	2.4
Yb	1.60	1.62	2.1	2.4	2.3	4.1	2.1	5.1	6.8	3.6	3.9	4.5	4.0	3.4	1.76	3.4	4.0	2.7	4.2	1.68	3.4	5.0	3.5	6.3	2.6
Lu	0.28	0.26	0.34	0.39	0.36	0.42	0.32	0.65	0.61	0.56	0.63	0.70	0.64	0.32	0.33	0.50	0.63	0.42	0.67	0.29	0.56	0.81	0.56	1.06	0.42
LREE	68.46	79.45	89.51	81.77	86.10	130.47	78.83	281.99	231.59	221.88	196.14	187.50	227.79	114.23	210.66	207.23	275.56	198.43	127.58	83.65	82.08	128.40	89.21	181.47	79.58
HREE	10.61	10.55	13.38	14.91	13.80	19.05	12.14	35.11	28.25	20.32	24.11	24.00	27.28	14.09	14.68	23.15	28.36	20.18	23.43	11.42	16.51	25.42	18.23	34.97	13.26
LREE/ HREE	6.45	7.53	6.69	5.48	6.24	6.85	6.49	8.03	8.20	10.9	8.13	7.81	8.35	8.11	14.35	8.95	9.72	9.84	5.45	7.33	4.97	5.05	4.89	5.19	6.00
∑REE	79.08	90.00	102.89	96.68	99.90	149.52	90.97	317.10	259.84	242.20	220.25	211.49	255.07	128.32	225.34	230.38	303.92	218.61	151.00	95.07	98.60	153.81	107.44	216.44	92.84
La/Sm	4.04	5.30	3.83	3.63	3.71	6.20	4.71	7.28	6.23	7.42	5.35	6.21	4.38	4.64	7.29	4.58	6.38	5.79	3.61	4.06	4.25	3.69	3.78	4.06	4.76
Gd/Yb	1.98	2.01	1.99	1.78	1.83	1.33	1.70	2.42	1.18	1.62	1.77	1.42	2.25	1.19	3.25	2.27	2.31	2.47	1.49	2.16	1.13	1.26	1.33	1.45	1.32
La/Yb	8.30	11.87	8.40	6.19	6.85	9.09	8.40	18.76	8.76	13.82	10.24	10.11	11.08	6.57	31.12	12.05	16.49	16.41	5.55	9.18	4.64	4.66	5.30	5.93	6.59
La/Co	1.08	0.84	0.82	0.99	0.59	2.52	2.30	9.14	4.24	4.58	3.85	1.73	4.58	2.56	6.11	1.87	9.71	1.55	2.25	1.97	3.34	2.32	4.11	2.64	3.15
La/Sc	0.81	1.14	0.89	0.71	0.77	2.41	0.85	13.61	5.37	3.17	3.03	3.45	2.29	1.94	4.64	2.48	3.07	3.02	1.51	1.37	1.77	1.74	1.72	2.13	1.81
Y/Ho	28.92	28.94	28.60	29.44	29.82	34.60	28.23	40.09	30.54	28.23	29.55	29.72	29.09	28.76	27.57	29.53	28.12	29.21	28.93	28.94	31.15	29.88	30.57	30.50	29.30
$(Gd/Yb)_N$	1.19	1.22	1.16	1.07	1.06	0,80	1.02	1.45	0.69	0.96	1.07	0.85	1.33	0.72	1.93	1.35	1.39	1.50	0.88	1.28	0.67	0.76	0.78	0.87	0.78
Dy_N/Sm_N	0.94	0.86	0.89	1.05	0.98	0.84	0.92	0.76	0.79	0.89	0.95	0.96	0.81	0.74	0.55	0.76	0.82	0.79	1.06	0.89	1.22	1.13	1.07	1.10	1.03
La_N/Yb_N	0.81	1.15	0.80	0.60	0.65	0.87	0.82	1.82	0.84	1.32	0.99	0.97	1.07	0.66	3.03	1.17	1.62	1.61	0.53	0.89	0.45	0.45	0.51	0.58	0.64
Gd_N/Yb_N	1.19	1.22	1.16	1.07	1.06	0.80	1.02	1.45	0.69	0.96	1.07	0.85	1.33	0.72	1.93	1.35	1.39	1.50	0.88	1.28	0.67	0.76	0.78	0.87	0.78
$(La/La^*)_N$	0.86	1.11	0.86	0.95	0.88	1.21	1.09	1.12	0.98	0.99	0.77	0.92	0.82	0.82	1.23	0.79	0.91	0.93	0.83	0.90	0.84	0.80	0.90	0.85	1.10
$(Pr/Pr^*)_N$	1.07	1.05	1.07	1.02	1.00	1.18	1.03	1.45	1.14	0.93	1.08	1.10	1.06	1.07	0.99	1.09	1.09	1.04	1.02	1.00	1.02	1.03	1.11	1.13	0.97
$(Ce/Ce^*)_N$	1.07	0.93	1.08	1.09	1.09	0.89	0.97	0.89	0.94	0.91	1.05	0.95	1.08	1.05	0.84	1.08	0.94	0.96	1.10	1.07	1.06	1.10	1.06	1.07	0.94
δCe	1.06	0.77	0.80	0.98	1.00	0.31	0.84	0.07	0.23	0.41	0.38	0.32	0.33	0.65	0.31	0.34	0.23	0.36	0.67	1.02	1.00	0.66	0.68	0.33	1.00

VI. Discussion

The obtained geochemical data are used to help characterize and classify each sampled mudrock and Quaternary material. They are used to trace the provenance of deposited materials, and determine their source rock composition. Pre-depositional and syn-depostional processes and conditions are also developed.

A. Mudrocks

a) Characteristization and classification

The trace and rare earth elements concentrations in mudstones, and schistose marls from the Babouri-Figuil Basin show differences; with some samples being much chemically enriched than others. They are either higher, close, or lower than the average values in Upper Crust presented in [44]. Within the trace elements suites (in a general aspect), relatively highly concentrated elements are Ba, Sr, Zn, Zr, and V. Stronstium is a distinctive element between schistose marls and mudstones, as it is highly concentrated in these rocks than in mudstones. Other distinctive features are the Zr, Ba, Zn, and V contents. The Zr content is relative higher in Mayo Tafa mudstones than in Dafang mudstones and Mayo Figuil schistose marls. Barium content is very low in MFL1-2, than in other mudrocks, although some schistose marls have relative low Ba. Vanadium and Zn is relatively higher in Danfang mudstones and many schistose marls. These trace elements variations lead to the following classification : (1) relatively high Sr and low Ba-Zn-Zr-V schistose marls; (2) relatively low Sr and high Ba-Zn-Zr-V schistose marls; (3) relatively high Ba-Zr and low Zn-V mudstones; and (4) relatively low Ba-Zr and high Zn-V mudstones.

The heterogeneity and extreme variation of rare earth element concentrations has lead to the distinction of: relatively high REE mudrocks ($\sum$REE > 214 ppm) (all mudstones from Mayo Tafal and one schistose marls: M'FL4-1) and relatively low REE mudrocks ($\sum$REE $\leq$ 81 ppm) (some schistose marls: MFL3-1, MFL1-2, MFL4-3, MFL5-3…). Those with $\sum$REE ranging from $\leq$ 188 to 135.10 ppm form an intermediate group (all mudstones from Dafang and some schistose marls). The total rare earth element concentrations in the studied mudrocks are in some case more than that of the North American Shale Composite (NASC) (173.21 ppm: [45]). The plotted data in $(Ce/Ce^*)_N$ versus $(Pr/Pr^*)_N$ field discriminative diagram of [46] (Fig. 10) distinguish four groups including those plotted in: (1) field I (one Mayo Tafal mudstone and many schistose marls); (2) field IIa (two Mayo Tafal mudstones) ; (3) field IIb (all Dafang mudstones); and (4) field IIIb (two schistose marls).

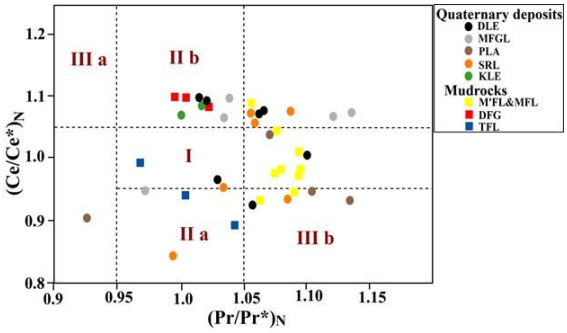

Fig 10 : Cross plots for Babouri-Figuil mudrocks and fine-grained-rich Quaternary deposits in [46]$(Pr/Pr^*)_N$ versus $(Ce/Ce^*)_N$ binary diagram (I: neither Ce_N no La_N anomaly; IIa : positive La_N anomaly, no Ce_N anomaly; IIb : negative La_N anomaly, no Ce_N anomaly; IIIa: positive Ce_N anomaly; IIIb: negative Ce_N anomaly).

b) Provenance and source rock(s)

Trace and rare earth element compositions in the Babouri-Figuil mudrocks show some similarities and differences probably due to the existance of multiple sources. Those with similar features (overlapsing normalized patterns : Figs. 6-9 ; plotted in the same field : Fig. 10 and plotted very close: Fig. 11) can be of the same provenance. Those with different features are problably of different origins. The Cr and Ni contents, Cr/Ni, Y/Ni, La/Sc, Th/Sc, Th/Co, Cr/Th, and $(Gd/Yb)_N$ ratios, and REE patterns have being succesfully used to constrain the provenance of mudstones and other lithified clastic sediments (e.g.,[24, 44, 47-51]). For [52] lithified fine-grained clasts (shales) from ultrabasic roks have their Cr contents (> 150 ppm), Ni (> 100 ppm) and low Cr/Ni ratios (1.3-1.5). The Cr and Ni contents and Cr/Ni ratios in the Babouri-Figuil mudrocks are for: Dafang mudstones (Cr: 54-89 ppm, Ni:41-52 ppm; Cr/Ni:1.4-1.8); Mayo Tafal mudstones (Cr:50-62 ppm; Ni:24-39 ppm, Cr/Ni: 1.59-2.17); and Mayo Figuil schistose marls (Cr: 9.6-67; Ni: 5.7-68 ppm ; Cr/Ni : 0.69-1.67). These values are dominanly less than those of clasts sorted from ultramafic rocks (cf. [52]), and therefore, show no ultramafic contribution. They could be from felsic and/or mafic sources, as their features (high to low LREE/HREE, and negative to no Eu anomalies) are compatible with those of terrigneous sediments sorted from these rocks types presented in [49-51]. This felsic to mafic sources are also shown in Table 5, some are within the range limit in sediments from felsic and mafic rocks. Mafic contrubutions are also supported, as the Y/Ni ratios ($\leq$ 0.8) for some samples are within the value for mafic source sediments proposed in [24].

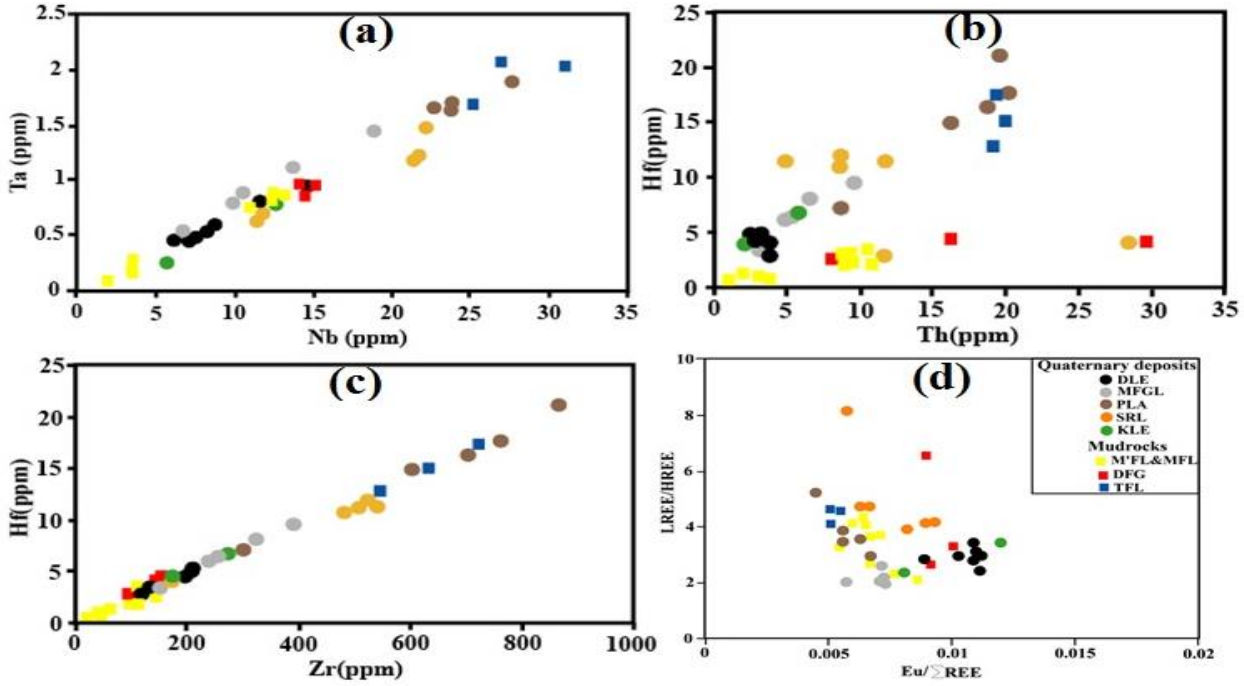

Fig. 11 : Simple bivariate plot diagrams of trace elements and REEs of the Babouri-Figuil mudrocks and fine-grained-rich Quaternary deposits, showing some grouping.

The La/Sc, Th/Sc, Th/Co, and Cr/Th ratios for mudrocks from Babouri-Figuil compare to the average values in Upper Continental Crust (UCC), Low Continental Crust (LCC) and Oceanic Crust (OC) proposed by [53] (Table 5), are much closer to those of Upper Continental Crust. This closeness shows that the studied mudrocks are from a Upper Continental Crust. For [44], the $(Gd/Yb)_N$ ratio is less than 2 (< 2.0) in Post-Archean strata and more than 2 (> 2.0) in Archean strata. Excepting that of DFG1-1 (> 2.0), the $(Gd/Yb)_N$ ratio (0.69-1.79) in the studied mudrocks are less than 2. They are mainly from Post-Archean strata with just one sample from Archean strata. The basement rocks in Babouri-Figuil (embrechite gneiss, muscovite-bearing gneiss, marbles, calc-schists, chlorite schists, serite schists, upper mica-schists, quartzites, alkaline granitoids) are Post-Archean rocks (part of the Cameroon Mobile Belt) [36, 43]. These post-Achean rocks can be the sources of part of the consolidated materials forming the studied mudstrocks.The existance of Archean strata feature presented by one Dafang mudstone (DFG1-1) is difficult to correlate locally, as published data are lacking, but could be attempted in a regional scale. DFG1-1 can be originated from inherited Archean rocks associated to the Cameroon Mobile Belt, as Archean inheritance has been proven within some rocks of the Cameroon Mobile Belt (example within metamorphic rocks in Meiganga, Adamawa Region of Cameroon :[54, 55].

Table 5 : Trace and REEs ratios of the Babouri-Figuil mudrocks compare to those of UCC, LCC, and OC from [53] and those of felsic and mafic source sediments from [69]

Element Ratios	UCC	LUC	OG	Mayo Dafang Mudstones	Mayo Tafal Mudstones	Mayo Figuil Schistose marls	Range for sediment from mafic source	Range for sediment from felsic source
La/Sc	2.70	0.30	0.10	1.30-1.87	2.76-3.76	1.21-6.11	0.43-0.76	2.50-16.3
La/Co	1.76	0.33	/	0.7-1.04	2.7-4.2	1.08-3.33	0.14-0.38	1.80-13.8
Th/Sc	0.97	0.03	0.94	0.71-1.88	1.25-151	0.21- 0.96	0.05-0.22	0.84-20.5
Th/Co	1.07	0.03	0.01	0.28-1.31	1.28-1.66	0.19- 0.73	0.04-1.14	0.67-19.4
Cr/Th	7.76	109.5	/	1.9-10	2.5-3.3	4.02-10.32	25-500	4.0-15.0

The source(s) of the Babouri-Figuil mudrocks were determined in [48] La/Th versus Hf (Fig. 12a) and Co/Th versus La/Sc (Fig. 12b) discrimination diagrams. Plots fall in different fields which support the heterogeneity of the origin of deposited and consolidated materials. In Fig. 12a, (1) two schistose marls fall in andesite arc source field, two, in mixed felsic-basic source field and six others, out of all the fields; and (2) mudstones from Mayo Tafal and Dafang fall out of different fields. The differences are also visible in Fig. 12b with must schistose marls plots fall between andesites and felsic volcanic rocks, which suggests contributions from andesitic and felsic rocks. Mudstones from Mayo Tafal are much close to felsic volcanic rocks, which suggests contributions from felsic volcanic rocks. Those from Dafang show much scattered plots (one being close to andesites, one close to felsic

volcanic rocks, one being very far). Part of their source materials could be originated from andesitic rocks and others, from felsic volcanic rocks. Other diagram used to determine sediment's source rock(s) type and nature is the La/Yb versus ∑REE binary diagram of [47] (Fig. 13), in which the studied mudrocks are plotted in different fields. Within schistose marls suites, three samples are plotted in calcareous mudstones field (suggests contributions from in calcareous mudstones); two samples, within the intersection region of alkaline basalts and sedimentary rocks (suggests contributions from sedimentary and alkaline basaltic rocks); and five samples, within the intersection region of continent tholeiitic basalts and sedimentary rocks (suggests contributions from sedimentary and continent tholeiitic basaltic rocks). Mayo Tafal mudstones are plotted within the intersection region of alkaline basalts and sedimentary rocks. This suggests contributions from sedimentary and alkaline basaltic rocks. Dafang mudstones fall in three different zones: (1) in sedimentary rocks field (suggests contributions from sedimentary rocks); (2) within the intersection region of continental tholeiitic basalts and sedimentary rocks (suggests contributions from sedimentary and continent tholeiitic basaltic rocks); and (3) in continental tholeiitic basalts (suggests contributions continent tholeiitic basaltic rocks).

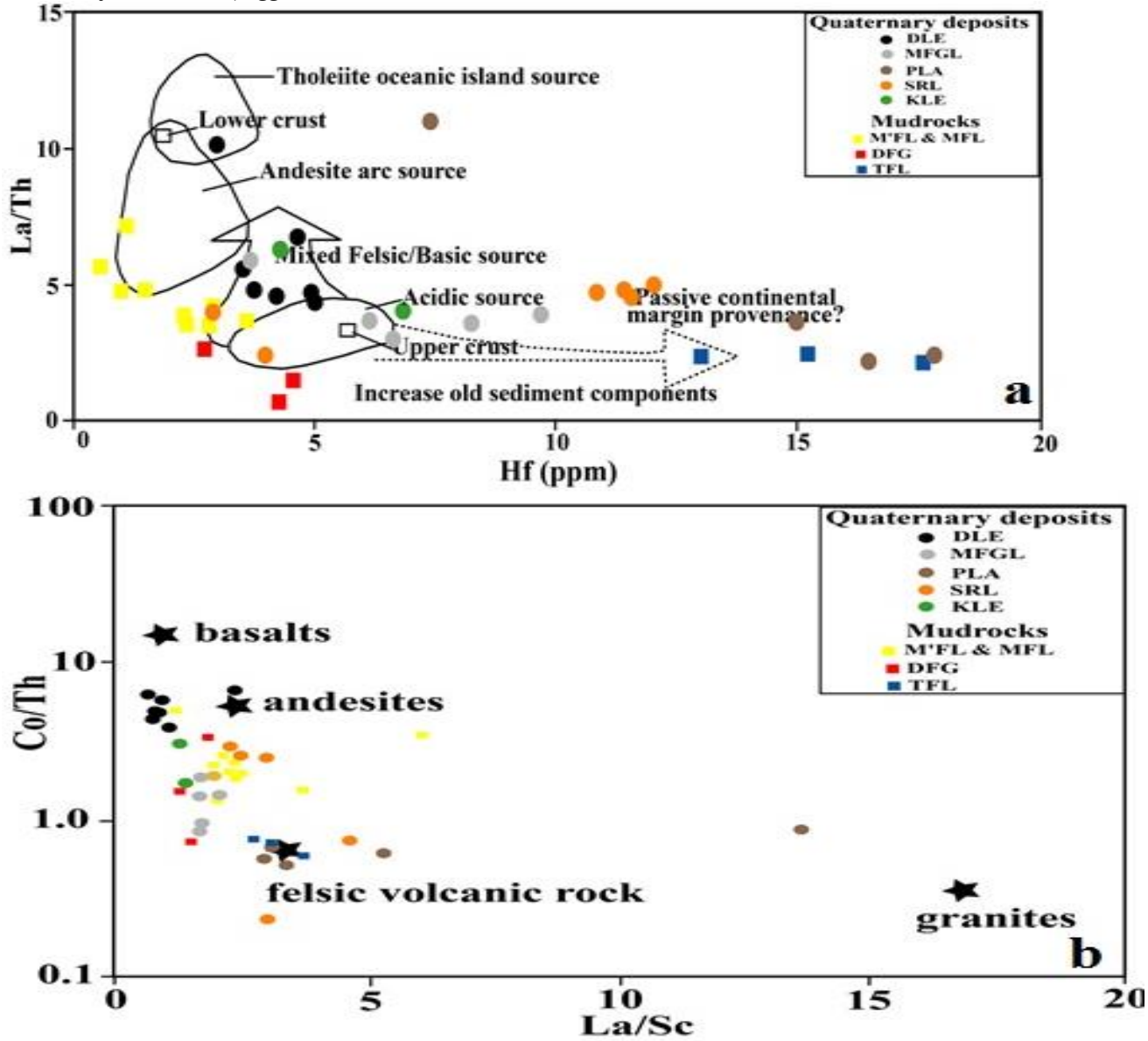

Figure 12: Source and compositional discrimination of the Babouri-Figuil mudrocks and fine-grained-rich Quaternary deposits, data plotted in [48].

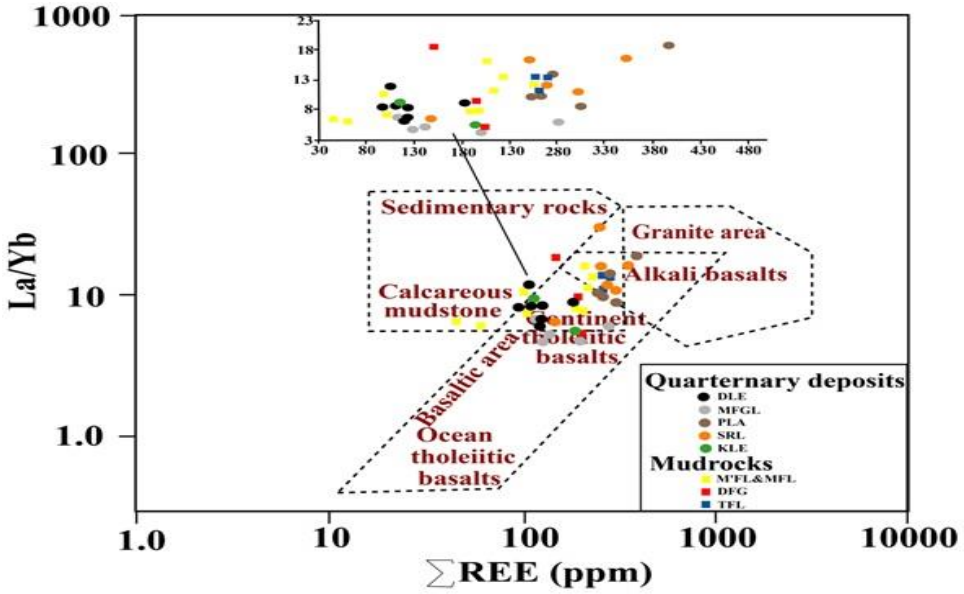

Fig. 13 : Plots for the Babouri-Figuil mudrocks and fine-grained-rich Quaternary deposits in [68] ∑REE versus La/Pr binary diagram.

c) Tectonic setting and depositional conditions

The tectonic setting in the area of creation of a sedimenatry basin and the depositional conditions of host deposits can be assessed by analyzing some trace and rare eath elements in sedimentatry rocks found in the basin (e.g., [2, 29, 32]). The plotted data for Babouri-Figuil mudrocks in [32] Th-Co-Zr/10 and La-Th-Sc ternary diagrams (Fig. 14) show that four mudstones (two from Dafang and two Mayo Tafal) and five schistose marls from Mayo Figuil are plotted in passive continental margin field. This suggests that Babouri-Figuil was probable a passive continental margin during the deposition sediments source of main of the mudrocks. They could be sedimentary rocks originated from the compaction fine-grained sediments deposited and transformed after the continental Cretaceous opening of the Babouri-Figuil Basin whose creation is related to that of the Benue Trough [34]. One mudstone from Mayo Tafal fall in Continental and oceanic island arc field. This suggests that Babouri-Figuil was a continental-oceanic island arc during the deposition of this rock's fine-grained siliciclastic sediments.

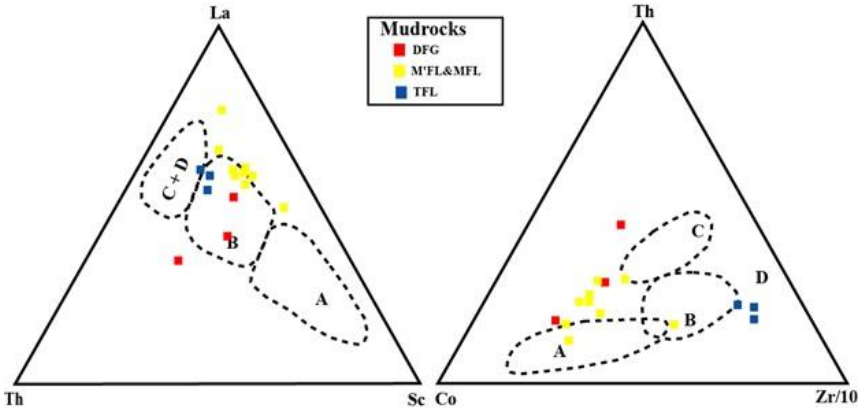

Fig. 14 : Tectonic discrimination plots for the Babouri-Figuil mudstones in [29] ternary diagrams (a: La–Th–Sc and b: Th–Co–Zr/10). A = oceanic island arc; B = continental island arc; C = active continental margin; D = passive margin

The V/(V+Ni), U/Th, V/Cr, and Ni/Co ratios, authigenic U (AU), δU, and Ce anomaly ($\delta Ce = Ce_N / (La_N \times Pr_N)^{1/2}$ have been used as indicators of depositional conditions of siliciclastic fine-grained sedimentary rocks (e.g., [56-60]). For [2] and [56] in euxinic conditions the V/(V+Ni) ratio is > 0.84, ranging from 0.6.0 to 0.84 when the conditions are anoxic, and from 0.4 to 0.6 when the conditions are dysoxic. The V/(V+Ni) ratios for those mudrocks range from 0.67 to 0.77, which are within the limit characterizing anoxic conditions proposed in [2] and [56]. The U/Th > 1.25 reflect strongly reducing conditions, ranging from 0.75 to 1.25, and represents a reducing

condition; and a mean oxic condition, when U/Th < 0.75 [57]. The U/Th ratios (0.05 to 0.17) for Dafang mudstones and (0.15 to 0.18) for Mayo Tafal mudstones suggests oxic conditions. The U/Th ratios (0.19 to 1.36) for Mayo Figuil schistose marls suggest oxic to strong reducing environments. In addition, for [57], the V/Cr and Ni/Co ratios in an oxic environment are < 2.0 and < 5.0, respectively, and > 2.0 to 4.25 and > 5.0 in a reducing environment. The V/Cr and Ni/Co ratios are respectively, 1.2 to 1.6 and 1.7 to 1.9 for Dafang mudstones, 1.3 to 1.4 and 1.6 to 2.71 for Mayo Tafal mudstones, 1.5 to 2.91 and 1.17 to 3.88, for Mayo Figuil schistose marls. Those for the Dafang and Mayo Tafal mudstones suggest an oxic environment. Those of Mayo Figuil schistose marls show oxic to anoxic conditions. The AU (>12 ppm) and δU (< 1.0) suggest a strongly reduced condition and an oxic condition, when AU (< 5 ppm) and δU (> 1.0) [59, 61]. For [58], the δCe > 1 indicates an oxic condition; and less than 1.0, when the condition is anoxic. Dafang mudstones with AU (-5.0 to -4.5 ppm), δU (0.24-0.67), and δCe (1.08-1.11) suggest dominantly oxic conditions. Mayo Tafal mudstones with AU (-3.57 to -3.0 ppm), δU (0.63-0.69), and δCe (0.89-1.0) show oxic to anoxic conditions. Mayo Figuil schistose marls with AU (-1.33 to 1.96 ppm), δU (0.74-1.60), and δCe (0.78 to 1.10), suggests oxic to anoxic conditions.

d) Paleoclimatic and Paleosanility interpretations

Trace element contents in fine-grained siliciclastic sedimentary rocks have been used for paleoclimatic interpretations (e.g., [62, 63]). The most used elements are Ga, Rb, Cu, and Sr whose concentration in a fine-grained lithified sedimentary rock is related to the nature of their host-mineral and pre-existing climatic conditions during sediment's deposition [62]. The Ga/Rb and Sr/Cu ratios have been successfully used to interpret pre-existing climatic conditions during the depositional phase of fine-grained clastic sediments [2, 60, 62]. For [60] deposited sediments show high Ga/Rb and low Sr/Cu ratios when the climatic conditions are warm and humid. The Ga/Rb and Sr/Cu ratios for the Babouri-Figuil mudrocks range from 0.29 to 0.39 and 4.04 to 8.2 for Dafang mudstones, 0.18 to 0.23 and 8.0 to 15.0 for Mayo Tafal mudstones and 0.29 to 0.39, and 8.0 to 575.14 for Mayo Figuil schistose marls. The only sample (DFG3-1) with Sr/Cu ratios (≤ 5) may reflect a humid environment, and the rest with ratio (> 5) could typify an arid environment, if based on [60] classification (1.3 ≤ Sr/Cu ≤ 5 for humid climate and Sr/Cu > 5 for arid environment). As shown in Fig. 15 (Cross plot diagram of Sr/Cu versus Ga/Rb ratios showing paleoclimatic variation), just one sample (DFG3-1) is plotted in a warm-humid zone; three from Mayo Tafal, fall in a cool-arid zone, and the other samples (two from Dafang and all those from Mayo Figuil), fall in warm-arid zone. It can be suggested that Babouri-Figuil was warm and humid (during the depositional period of DFG3-1); cool and arid (during the deposition mudstones in Mayo Tafal); and warm and arid (during the deposition sediments source of the Mayo Figuil schistose marls and two Dafang mudstones : DFG1-1 and DFG5-1).

Sr/Ba ratios have been used to evaluate paleosalinity and differentiate Lake and marine sediments [14, 64]. For [64], the Sr/Ba ratio in Lake deposits is less than 0.6, ranging from 0.8 to 1.0 in marine sediments. The Sr/Ba ratios ranging from 0.38 to 0.76 in Dafang mudstones and 0.26 to 0.31 in Mayo Tafal mudstones are dominantly within the range limit proposed for Lake deposits. It may be suggested that the deposition of Mayo Tafal and Dafang mudstones took place in a Lake environment. The Sr/Ba ratios (0.73 to 6.33) for Mayo Figuil schistose marls are above the maximum value for Lake deposits. One value (0.93: MFL2-2) is within range limit for sea deposits, which could suggest deposition in a marine environment. For [14], the Sr/Ba ratio (> 1.0) is related to sea water to brackish water, if ranging from 0.6 to 1.0, and to fresh water, if less than 0.6. The Sr/Ba ratios < 0.6 for Mayo Tafal and two Dafang mudstones (DFG3-1 and DFG5-1) suggests fresh water deposition. The Sr/Ba ratios (0.74-0.93) for one Dafang mudstone (DFG1-1) and two schistose marls (M'FL1-1 and MFL2-2) from Mayo Figuil suggests brackish water depositions. A marine depositional environment is suggested for the other Mayo Figuil schsitose marls with Sr/Ba ratios > 1. In summary, the paleosalinity of water during the sedimentation of the Babouri-Figuil mudrocks could be: (1) fresh water for Mayo Tafal mudstones and two Dafang mudstones; (2) brackish water for one mudstone from Dafang and two schsitose marls from Mayo Figuil; (3) sea water for most Mayo Figuil schistose marls.

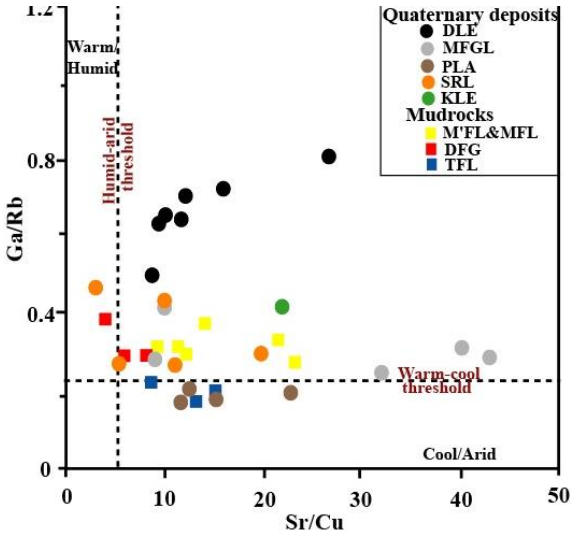

Fig. 15 : Cross plot diagram of Sr/Cu versus Ga/Rb ratios for the Babouri-Figuil mudrocks and fine-grained-rich Quaternary deposits showing paleoclimatic variation.

B. Quaternary deposits

a) Characteristization and classification

Trace and rare earth element composition in Babouri-Figuil fine-grained-rich Quaternary deposits is heterogenous with some similarities that help to differentiate them. This variation, observed for samples from the same pit, can characterize different source(s) and depositional history. In a global point of view, samples from Délélé, Mayo Figuil, and Kolé are geochemically less enriched than those from Pomla and Sorawel. This clearly differentiate them; with those in Pomla and Sorawel classified as relatively-high trace and REE fine-grained- rich Quaternary deposits, and those in Délélé, Mayo Figuil, and Kolé considered as relatively-low trace and REE Quaternary deposits. The highest elemental concentrations are those of Ba, Sr, Zr, Rb, and V. These elemental contents are dominantly different to those published by [65] for Lokoundje alluvial deposits (south of Cameroon) which compare with the Babouri-Figuil Quaternary deposits, are relatively highly enriched in Ba, but depleted in Zr and Sr. In the studied samples LREE is generally highly concentrated than HREE which is common in fine-grained deposits (cf. [66]). With the high variation of REE contents (∑REE: 79-318 ppm) samples have been grouped into three : (1) those with very low REE (∑REE: 79-108 ppm); (2) those with low REE (∑REE: 109-151 ppm); and (3) those with slightly high REE (∑REE: 216-318 ppm). Three samples (MFGL1, MFGL5, MFGL9) from Mayo Figuil, one from Kolé (KLE4), and nearly all samples (excepting DLE14) from Délélé fall within the group 1. One sample from Kolé (KLE1), Sorawel (SRL2), and Mayo Figuil (MFGL3) fall within the group 2. All samples from Pomla and nearly all from Sorawel (excepting SRL2) and one from Mayo Figuil (MFGL6) fall within the group3. The plotted data in $(Ce/Ce^*)_N$ versus $(Pr/Pr^*)_N$ field discriminative diagram of [46] (Fig. 12) distinguish five subgroups excluding those in : (1) field I (one from Délélé and one from Sorawel); (2) field IIa (one from Sorawel and one from Mayo Figuil); (3) field IIb (two from Délélé, two from Kolé and two from Mayo Figuil); (4) much plots in field IIIa.

b) Provenance and source rock(s)

The Th, Sc, Co, Cr, Ni, Y, and LREE concentrations, and the following ratios Th/Co, La/Co, LREE/HREE, Th/Sc, La/Sc, Cr/Th, Cr/Ni, Y/Ni and $(Gd/Yb)_N$ ratios have been used to discriminate the provenance of unlithified siliciclastic fine-grained sediments and sedimentatry rocks (e.g., [2, 24, 44]). These same parameters have been used to infer the provenance of fine-grained-rich levels in Quaternary deposits found in the Babouri-Figuil Basin. The La/Co, Th/Sc, La/Sc, Cr/Th ratios of the studied sediments compare to the average values in Upper Continental Crust (UCC), Low Continental Crust (LCC) and Oceanic Crust (OC) (Table 6) show closness with those of the Upper Continental Crust (UCC), and, suggest an Upper Continental Crust origin. For [44] the $(Gd/Yb)_N$ ratio is less than 2 in Post-Archean strata, and, more than 2 in Archean strata. The $(Gd/Yb)_N$ ratios for the studied sediments varying from 0.6 to 1.2, indicate provenance from Post-Archean strata. Post-Archean intrusive, metamorphic, and sedimentary rocks crop out around the studied Quatenary deposits, upstream of the draining streams, or are underlain by the sediments. They could have feed these sediments with detritus.

Elements such as La, Th, and LREE enrichements in sediment indicate a felsic source; Sc enrichement indicates mafic; Cr and Ni enrichement indicate ultramafic to mafic sources [52]. Fine-grained-rich sediments from Mayo Délélé enclose La (13-37 ppm), LREE (68-131 ppm), Th (2.8-3.7 ppm), Sc (15-21 ppm), Cr (41-59 ppm), Ni (18-42 ppm) and (LREE/HREE : 5-7). Those from Pomla enclose La (40-96 ppm), LREE (187-282 ppm), Th (8-20 ppm), Sc (7-16 ppm), Cr (31-61 ppm), Ni (16-32 ppm) and (LREE/HREE : 7-11). Sediment from Sorawel enclose La (23-57 ppm), LREE (114-276 ppm), Th (5-28 ppm), Sc (11-22 ppm), Cr (45-138 ppm), Ni (20-112 ppm) and (LREE/HREE : 8-15). Those from Kolé enclose La (15-23 ppm), LREE (83-128 ppm), Th (2-6 ppm), Sc (5-16 ppm), Cr (10-29 ppm), Ni (6-20 ppm) and (LREE/HREE : 5-10). Sediments from Mayo Figuil enclose La (15-38 ppm), LREE (79-182 ppm), Th (3-10 ppm), Sc (9-19 ppm), Cr (11-21 ppm), Ni (7-25 ppm) and (LREE/HREE : 4-8). The above values show extreme variations from one sample to another, and from one pit to another; which show that different rock-types feed the Babouri-Figuil fine-grained-rich quatenary deposits.

Fine-grained-rich Quatenary materials from Délélé encloses low Cr and Ni contents, which indicate no contribution from ultramafic-ultrabasic source. The La, LREE, Th, Y, Ni, Cr, and Sc contents, and LREE/HREE ratios suggest contributions of both felsic and mafic sources. The obtained La/Co, Th/Sc, La/Sc, Y/Ni, and Cr/Th ratios are in some case closer to those of sediments from mafic rocks and those of sediments from mafic rocks (Table 6). The low La, LREE, and Th contents in the studied sediments can be due their low concentrations in their source rocks. Their felsic and mafic provenance is shown in Fig. 12a with most plots falling in mixed felsic-basic source. Their plots near andesites (Fig. 12b), can shows contributions from rocks with an andesitic composition. Their plots mainly falling in a zone including continent tholeiitic basalts and sedimentary rocks (Fig. 13) supports contributions from basic and sedimentary rocks. The studied samples are in most cases plotted very close in Figs. 10-13; and, the normalized patterns (Figs. 8a and 9a) showing almost the same behavior, which could suggest the same provenance for most of the detritus.

Pit dug in Pomla is also made up of relatively poored Cr and Ni fine-grained-rich quatenary materials; which also show no ultrmafic source contribution, but contributions of mainly felsic sources. Their felsic sources are confirmed in Table 6, with their obtained La/Co, Th/Sc, La/Sc, Cr/Th ratios being within the range of sediments sourced from felsic rocks. The relatively high LREE contents in these sediments can show the enrichement of these elements in their source rocks. Their plots falling out of all source discriminatìon fields in Fig. 12a, but much closer to felsic volcanic rocks in Fig. 12b, support their felsic provenance. The studied samples

normalized patterns plots in Figs. 8b and 9b are different, and, thier plots in Figs. 12, 13 and 15 are scattered. This shows that the studied samples are from different sources. The studied samples are plotted in three different zone in Fig. 13. One plot falls in a zone including granite area and alkali basalts (Fig. 13), which could show contributions from both granitic and alkali basaltic rocks. One other plot falls in an area including sedimentary rocks and alkali basalts, which suggest contributions from these two rock groups. Three other plots fall on the dividing line between alkali basalts, and continent tholeiitic basalts, which could show contributions from alkali basaltic and tholeiitic basaltic rocks.

Fine-grained-rich sediments from Sorawel are relatively poored to slightly enriched Cr and Ni. The relatively high Ni and Cr content in some samples; could show some ultrabasic contributions, as the Ni content in one sample (SRL8) is more than the mean value (Ni > 100 ppm) in sediments from ultrabasic rocks (cf. [52]) and Y/Ni ratio (0.3) is less than 0.8 for sediment from ultrabasic rocks (cf. [24]). Their La, LREE, Th, and Sc contents and LREE/HREE ratios suggest contributions of predominantly for felsic source(s), with just little contribution from mafic source(s).The predominance of felsic source(s) contributions are shown in Table 6, with the La/Co, Th/Sc, La/Sc, Cr/Th ratios being much within the range limit of those of felsic source sediments. Felsic contributions is also show in Fig. 12a, as one plot is almost in mixed felsic-basic source, and one in acidic source field; and in Fig. 12b, with some plots falling close to andesites. The studied samples normalized patterns (Figs. 8c and 9c) show different behavior, and, thier plots in Figs. 10-13, are scattered. From their plots in Fig. 13, five groups can be distinguished: (1)one sample plotted in a zone coverying alkali basalts, and granite, suggests contribution from granitic and alkali basaltic rocks; (2) one sample plotted on the deviding line between a zone including sedimentary rocks and granite area, suggests contribution from sedimentary and granitic rocks; (3) one sample plotted in a zone including continent tholeiitic basalt and sedimentary rocks, suggests contributions from sedimentatry and continent tholeiitic basaltic rocks; (4) one plot in continent tholeiitic basalt field, suggests contributions from tholeiitic rocks; and (5) three plots within the intersection region of alkaline basalts and sedimentary rocks, suggest contributions from sedimentary and alkaline basaltic origin.

Table 6 : Trace and REEs ratios of the Babouri-Figuil fine-grained-rich Quatenary deposits compare to those of UCC, LCC, and OC from [53] and those of felsic and mafic source sediments from [69]

Element Ratios	UCC	LUC	OC	Mayo Délélé	Mayo Louti (Pomla)	Mayo Sorawel	Mayo Kolé	Mayo Figuil	Range for sediment from mafic source	Range for sediment from felsic source
La/Sc	2.70	0.30	0.10	0.71-2.41	3.03-13.61	1.94-4.64	1.51 -1.37	1.72-2.13	0.43-0.76	2.50-16.3
La/Co	1.76	0.33	/	0.59-2.52	1.73-9.14	1.55-6.11	1.97-2.25	2.32-4.11	0.14-0.38	1.80-13.8
Th/Sc	0.97	0.03	0.94	0.15-0.24	1.23-1.50	0.42-1.31	0.22-0.38	0.31-0.48	0.05-0.22	0.84-20.5
Th/Co	1.07	0.03	0.01	0.14-0.24	1.13-1.90	0.34-4.14	0.31-0.57	0.54-1.14	0.04-1.14	0.67-19.4
Cr/Th	7.76	109.5	/	13.42-19.31	2.59-8.38	3.81-27.7	4.42-5.0	2.52-3.96	25-500	4.0-15.0

Fine-grained-rich sediments from Kolé enclose low Cr and Ni contents (which show no contribution from ultramafic source); but probably sourced from both felsic and mafic rocks, as their La, LREE, Th, and Sc contents (Table 3) and La/Co, Th/Sc, La/Sc, Cr/Th ratios (Table 6) are close to those of sediments from felsic and mafic rocks. Their felsic and mafic provenance are show in Figs. 12 and 13. In Fig. 12a, one sample is plotted in mixed felsic-mafic source field and the other one, plotted out of all fields. The studied samples normalized patterns have different behavior (Figs. 8d and 9d), and, thier plots in Figs. 10-13 are scattered, which can indicates different provenance. In Fig. 13, one sample is plotted on the deviding line between carbonaceous mudstone and continent tholeiitic basalts, which could suggest contritions from carbonate bearing mudstone, and continent tholeiitic basaltic rocks. The other sample plotted on the line separating the sedimentatry rocks area and continent tholeiitic basalts, could show contributions of predominantly from continent tholeiitic basaltic rocks.

Fine-grained-rich sediments from Mayo Figuil are depleted in Cr and Ni but have significant La, LREE, Th, and Sc contents. Their Th/Sc, La/Sc, and Cr/Th ratios in Table 6 are out the range limit for sediments sourced from felsic and mafic rocks. The La/Co and Th/Co ratios are mainly within the range limit for sediments sourced from felsic rocks (Table 6). The relavely high LREE and low Sc contents could support a felsic source for part of the studied sediments. The plotted data Fig. 12a fall in mixed felsic-mafic source zone, acid source zone, and out of all other fields. Part of the studied sediments was probaby sorted from felsic and mafic rocks with some of the felsic rocks being acidic. In Fig. 13, the studied samples are plotted in two main zones: (1) three samples are plotted within the intersection region of continent tholeiitic basalts zone and sedimentary rocks, which suggest contributions from continent tholeiitic basaltic and sedimentary rocks; and (2) three samples falls continent tholeiitic basalts, which could infer contributions from continent tholeiitic basaltic rocks.

c) Depositional conditions

The V/(V+Ni), V/Cr, and U/Th ratios and δU, have been used to infer the depositional conditions of the fine-grained-rich Quatenary sediments from Babouri-Figuil Basin. The V/(V+Ni) ratios range from 0.71 to 0.81 for

fine-graìned-rich deposits in Délélé, 0.73 to 0.75 for those in Pomla, 0.57 to 0.83 for those in Sorwel, 0.79-0.88 for those in Kolé, and 0.76 to 0.84 for those in Mayo Figuil. These values are generally within the range limit of values 0.6 to 0.84 for anoxic conditions for fine-grained sedimentary clastic rocks proposed by [2, 14, 59] with just one sample (SRL8 with V/(V+Ni): 0.57) representing euxinic or reducing conditions if based of [2] (V/(V+Ni) >0.5). It is therefore suggested that nearly all the studied sediments were deposited during reducing conditions. For [59] V/(V+Ni) ratios less than 1.0 indicate strongly reducing conditions. The V/Cr ratios range from 1.69 to 2.51 for fine-graìned-rich deposits in Délélé, 1.19 to 1.41 for those in Pomla, 1.23 to 2.29 for those in Sorawel, 2.58-4.59 for those in Kolé, and 2.07 to 4.18 for those in Mayo Figuil. For [67], the V/Cr > 4.25 for fine-grained terrigenous sedimentary rocks also indicates strong reducing conditions, if ranging from 2.0 to 4.5; and oxidative conditions, if less 2.0. Based on the [62] classification, reducing conditions can be suggested for most deposits in Délélé, Kolé, and Mayo Figuil and one sample from Sorawel (SRL7: 2.29), and oxidation conditions, for one sample in Délélé (DLE: 1.69), most samples in Sorawel and all samples in Pomla. The U/Th ratios range from 0.21 to 0.28 for samples from Délélé, 0.17 to 0.30 for those in Pomla, 0.10 to 0.40 for those in Sorawel, 0.22 to 0.38 for those in Kolé, and 0.27 to 0.35 for those in Mayo Figuil. These ratios are all within the range limit U/Th< 0.75 indicating oxidizing conditions proposed by [57], supporting oxic depositional conditons for those sediments.

d) Paleoclimatic interpretations

The Ga/Rb and Sr/Cu ratios, which were used as indicators to determine the paleoclimate of some fine-grained sediments [62, 68], have been used for fine-grained rich Babour-Figuil Quaternary deposits. The Ga/Rb ratio for deposits in Délélé ranges from 0.51 to 0.81, 0.18 to 0.21 for those in Pomla, 0.26 to 0.47 for those in Sorawel, 0.42 to 0.49 for those in Kolé, and 0.25 to 0.41 for those in Mayo Figuil (see Fig. 15). The Sr/Cu ratio for deposits in Délélé ranges from 8.51 to 26.19, 11.75 to 22.71 for those in Pomla, 2.79 to < 1165 for those in Sorawel, 21.90 to < 920 for those in Kolé, and 8.70 to 42.85 for those in Mayo Figuil. As proposed by [60], the Sr/Cu ratios indicate humid conditions ranging from 1.3 to 5.0, and more than 5.0 when the climate is arid. Excepting the value of SRL7 (Sr/Cu: 2.79), which is within values indicating a humid climate, all the other values are greater 5, suggesting arid climatic conditions. Most plots fall within arid-cool field in Fig. 15, indicating that Babouri-Figuil was characterized by variable climatic conditions: humid and warm during the deposition of SRL4; arid and cool during the deposition of all the fine-grained-rich deposits in Pomla; and arid and warm during the depositional of those in Délélé, Sorawel, Kole, and Mayo Figuil.

VII. Conclusions

The Babouri-Figuil mudrocks (mudstones and schistoses marls) are fine-grained rocks sourced from typical Upper Continental Crust and dominantly from post-Archean strata. Dafang mudstones are composed of materials probably sourced from felsic, andesitic, continental tholeiitic basaltic, and (or) sedimentary rocks. Mayo Tafal mudstones are made up of materials probably sourced from felsic volcanic, alkali basaltic, and sedimentary rocks. Schistose marls are composed of detritus probably originating from andesitic, continental tholeiitic basaltic, alkaline basaltic, and (or) sedimentary rocks. The detritus source of the studied mudrocks were mainly deposited within a passive continental margin. This deposition occurred under a range of oxidizing to reducing conditions. The climatic conditions during depositional periods were warm- humid, cool-arid, and warm-arid. The deposition of Mayo Tafal and Dafang mudstones was mainly in a lacustrine environment. The Mayo Figuil schistose marls were deposited in brackish to sea water.

The Babouri-Figuil fine-grained-rich Quaternary deposits are detritus sourced from Upper Continental Crust and post- Archean strata. Fine-grained-rich sediments in Délélé were probably sourced from felsic, mafic, and sedimentary rocks with some of the felsic and mafic rocks being basaltic and andesitic in composition. Those in Pomla were probably sourced from mainly felsic rocks with few contributions from mafic and sedimentary rocks. Those in Sorawel were predominantly sourced felsic rocks with few contributions from ultramafic, mafic, and sedimentary rocks. Fine-grained-rich sediments in Kole were sourced from felsic, mafic, and sedimentary rocks with tholeitic basaltic contributions. Those in Mayo Figuil were sorted from felsic, mafic, and sedimentary rocks with some of the mafic rocks being alkaline and tholeiitic basaltic in composition. The fine-grained sediments were deposits mainly in oxidizing to reducing conditions. The climatic conditions were warm and humid, cool and arid, and warm and arid during the depositional periods.

Acknowledgements

We thank PRESS NO&SW (Project on Soil and Subsoil Resources in the North and the South West Regions) for funding the field work. David Lentz helped edit an earlier version of this manuscript.

References

[1] Fang X, Peng B, Zhang K, Zeng D, Kuang X, Wu B, Tu X, Zhaoliang Song Z, Xiao Y, Yang Z, Xie W, Bao Z, Tan C, Wan D., Geochemistry of major and trace elements in sediments from inlets of the Xiangjiang and Yuanjiang River to Dongting Lake, China. Env. Earth Sci. https://doi.org/10.1007/s12665-017-7193-5., (2018).

[2] Xie G, Shen Y, Liu S, Hao W x., Trace and rare earth element (REE) characteristics of mudstones from Eocene pinghu formation and Oligocene huagang formation in XihuSag, east China sea basin: implications for provenance, depositional conditions and paleoclimate. Mar. Petrol. Geol. 1, 1-35.

[3] Balaram V., Rare earth elements: A review of applications, occurrence, exploration, analysis, recycling, and environmental impact. Geosci. Front. 10 (2019) 1285-1303.

[4] Kamgang P, Chazot G, Njonfang E, Ngongang NBT, Tchoua FM., Mantle sources and magma evolution beneath the Cameroon volcanic line: Geochemistry of mafic rocks from the Bamenda Mountains (NW Cameroon). Gondwana Res. 24 (2013) 727-741.

[5] Kanouo SN, Yongue FR, Ghogomu RT, Kouske PA, Njonfang E, Yomeun BS, Basua AAE Petro-geochemistry, genesis and

economic aspects of mafic volcanic rocks in the west and southern part of the Mamfe Basin (SW Cameroon, Central Africa). J. Geol. Geophy. DOI: 10.4172/2381-8719.1000298., (2017).

[6] Kanouo SN, Wang L, Kouske PA, Yomeun BS, Basua AAE., Petro-geochemistry, genesis and economic aspect of syenitic and mafic rocks in Mind if Complex, Far North Cameroon, Central Africa. Int. J. Geosci. 10 (2019) 1081-1114.

[7] Ominigbo OE, Ukwang EE, Okumoko DP, Ukpai UJ ., Petrogenesis and Tectonic Setting of the Basement Rocks around Irruan Area, Bamenda Massif, SE Nigeria. J. Geosci. Geom. 8(1) (2020) 35-44.

[8] Aliyari F, Rastad E, Goldfarb JR, Sharif AJ., Geochemistry of hydrothermal alteration at the Qolqoleh gold deposit, northern Sanandaj-Sirjan metamorphic belt, northwestern Iran: Vectors to high-grade ore bodies. J. Geochem. Expl. 140 (2014) 111-125.

[9] Hu H, Li WJ, Harlov ED, Lentz RD, McFarlane MRC, Yang HY ., A genetic link between iron oxide-apatite and iron skarn mineralization in the Jinniu volcanic basin, Daye district, eastern China: Evidence from magnetite geochemistry and multi-mineral U-Pb geochronology. Geol. Soc. Am. https://doi.org/10.1130/B35180.1., (2019).

[10] Kravtsova GR, Tauson LV, Goryachev AN, Makshakov SA, Yu K, Arsent EV, Lipko, VS SEM study of the surface of arsenopyrite and pyrite from the Natalkinskoe Deposit, Northeastern Russia. Geochem. Int. 58 (2000) 531–538.

[11] Ballouard C, Poujol M, Mercadier J, Deloule E, Boulvais P, Baele JM, Cuney M, Cathelineau M., Uranium metallogenesis of the peraluminous leucogranite from the Pontivy-Rostrenen magmatic complex (French Armorican Variscan belt): the result of long-term oxidized hydrothermal alteration during strike-slip deformation. Miner Deposita, DOI 10.1007/s00126-017-0761-5., (2017).

[12] Mavrogonatos C, Voudouris P, Berndt J, Klemme S, Zaccarini F, Spry GP, Melfos PG, Tarantola V, Keith A, Klemd M, Haase R., Trace elements in magnetite from the Pagoni Rachi porphyry prospect, NE Greece: Implications for ore genesis and exploration. Minerals, 9(12) (2019) 725.

[13] Jiao W, Yang H, Zhao Y, Zhang H, Zhou Y, Zhang J, Qilai Xie O., Application of trace elements in the study of oil-source correlation and hydrocarbon migration in the Tarim. Ener. Expl. Expl. 28(2010) 451-466.

[14] Li D, Li R, Zhu Z, Xu F., Elemental characteristics of lacustrine oil shale and its controlling factors of the palaeo-sedimentary environment on oil yield: a case from Chang 7 oil layer of Triassic Yanchang Formation in southern Ordos Basin. Acta Geochim, 37(2) (2018) 228-243.

[15] Graham EG, Kelley DK, Slack FJ, Koenig AE., Trace elements in Zn-Pb-Ag deposits and related stream sediments, Brooks Range Alaska, with implications for Tl as a pathfinder element. Geochem. Expl. Env. Anal. 9(2009) 19-37.

[16] Wang GJ, Cheng TJ, Wang DY., Experimental study on trace element method in surface geochemical prospecting for oil and gas. Petroleum Geology & Experiment (in Chinese with English abstract), 27(5) (2005) 544-549.

[17] Tang YP, Li DM, Chen JY, Wang GJ, Chen TJ ., The application of trace elements to geochemical exploration for oil and gas. Geophy. Geochem. Expl. 32 (2008) 350-353.

[18] Singh R, Kumar M, Venkatesh SA, Kurakalva MR, Syed HT, Reddy SGA., Assessment of potentially toxic trace elements contamination in groundwater resources of the coal mining area of the Korba Coalfield, Central India. Env. Earth Sci., 76(2017) 16. DOI 10.1007/s12665-017-6899-8

[19] Mandeng BPE, Bidjeck BML, Ekoa-Bessa AZ, Ntomb DY, Wadjou WJ, Doumo EPE, Bitom DL Contamination and risk assessment of heavy metals, and uranium of sediments in two watersheds in Abiete-Toko gold district, Southern Cameroon. Heliyon, https://doi.org/10.1016/j.heliyon.2019.e02591 ., (2019).

[20] Tehna N, Sababa E, Ekoa-Bessa ZA, Etame J Mine Waste and Heavy Metal Pollution in Betare-Oya Mining Area (Eastern Cameroon). Env. Earth Sci. Res. J. 6 (2019) 167-176.

[21] Cullers RL., The geochemistry of shales, siltstones, and sandstones of Pennsylvanian-Permian age, Colorado, USA: implications for provenance and metamorphic studies. Lithos, 51(2000) 181-203.

[22] Bhuiyan HAM, Rahman JJM, Dampare SB, Suzuki S (2011) Provenance, tectonics and source weathering of modern fluvial sediments of the Brahmaputra-Jamuna River, Bangladesh: Inference from geochemistry. J. Geochem. Expl. 111(2011) 113-137.

[23] Hofer G, Wagreich M, Neuhuber S ., Geochemistry of fine-grained sediments of the upper Cretaceous to Paleogene Gosau Group (Austria, Slovakia): Implications for paleoenvironmental and provenance studies. Geosci. Front. 4(2013) 449-468.

[24] Sharma A, Sensarma S, Kumar K, Khanna PP, Saini KN., Mineralogy and geochemistry of the Mahi River sediments in tectonically active western India: Implications for Deccan large igneous province source, weathering, and mobility of elements in a semi-arid climate. Geochim. Cosmochim. Acta, 104 (2013) 63-83.

[25] Tripathy RG, Singh KS, Ramaswamy V., Major and trace element geochemistry of Bay of Bengal sediments: Implications to provenances and their controlling factors. Palaeogeogr. Palaeoclimatol Palaeoecol. 397 (2014) 20-30.

[26] Bertrand S, Hughen, AK, lveda SJ, Pantoja S Geochemistry of surface sediments from the fjords of Northern Chilean Patagonia (44-47°S): Spatial variability and implications for paleoclimate reconstructions., Geochim. Cosmochim. Acta, 76(2012) 125-146.

[27] Rashid AS, Ganai AJ, Masoodi A, Khan AF., Major and trace element geochemistry of lake sediments, India: implications for weathering and climate control. Arab. J. Geosci. 8(2014) DOI 10.1007/s12517-014-1639-9.

[28] Bhatia MR., Rare earth element geochemistry of Australian Paleozoic graywackes and mudrocks: Provenance and tectonic control. Sediment. Geol. 45 (1985) 97-113.

[29] Bhatia MR, Crook KA., Trace element characteristics of graywackes and tectonic setting discrimination of sedimentary basins Contrib. Mineral. Petrol. 92 (1986) 181-193.

[30] Armstrong-Altrin JS, Verma SP., Critical evaluation of six tectonic setting discrimination diagrams using geochemical data of Neogene sediments from known tectonic settings. Sediment. Geol., 177 (2005) 115-129.

[31] Hu JJ, Li Q, Li J, Huang J, Ge DS Geochemical characteristics and depositional environment of the Middle Permian mudstones from central Qiangtang Basin, northern Tibet. Geol. J. 51(2016) 560–571.

[32] Bokanda EE, Fralick P, Ekomane E, Njilah IK, Bisse SB, Akono DF, Ekoa-Bessa AZ Geochemical characteristics of shales in the Mamfe Basin, South West Cameroon: Implication for depositional environments and oxidation conditions. J. Afr. Earth Sci. https://doi.org/10.1016/j.jafrearsci.2018.08.004., (2018).

[33] Tchouatcha SM, Tamfuh, AP, Sobdjou, KC, Mbesse, OC, Ngnotue, T., Provenance, palaeoweathering and depositional environment of the cretaceous deposits from the Babouri-Figuil and Mayo Oulo-Lere basins (North-Cameroon) during the Southern Atlantic opening: Geochemical constraints. J. Afr. Earth Sci. https://doi.org/10.1016/j.jafrearsci.2020.104052., (2021).

[34] Guiraud R, Maurin JC ., Early Cretaceous rifts of Western and Central Africa: an overview. Tectonophy, 213(1992) 153-168.

[35] Abolo NJA, Ngos III S, Ondoa BDA, Garcia B Fernanda-Sarmiento, M., Mbesse, O.C., Abolo MG, Eloung-Nna MD, Nkengfack EA, Ndjeng E, Qian, J (2014) Geochemical characterization and mineralogy of Babouri-Figuil Oil Shale, North-Cameroon. J. Surf. Eng. Mat. Advan.Techn. 4 (2014) 359-368.

[36] Schwoerer P ., Carte géologique du Cameroun au 1/500000, coupure de Garoua Est et notice d'explication. Direction des Mines et de la Géologie., (1962).

[37] Hervieu J L., existence de deux cycles climato-sédimentaire dans les monts Mandara et leurs abords (Nord-Cameroun). Conséquences morphologiques et pedogenétiques. C.R. Ac.Sc.L.264.serie D (1967) 2624-2627.

[38] Hervieu J., Le quaternaire du nord-Cameroun Schéma d'évolution géomorphologique et relations avec la pédogenèse. Cahier. O.R.S.T.O.M., sér. I'édol., 8(3) (1970).

[39] Ondoa BDA, Ngos III S, Ndjeng E, Abolo NJA, N'Nanga A., Contribution of the magnetic susceptibility to the characterization of the Babouri-Figuil Cretaceous Basin. Open J. Soil Sci. 4(2014) 272-283.

[40] Ngounouno I, Déruelle B, Guiraud R, Vicat PJ Magmatismes tholéiitique et alcalin des demi-grabens crétacés de Mayo Oulo-Léré et de Babouri-Figuil (Nord du Cameroun–Sud du Tchad) en domaine d'extension continentale. C. R. Acad. Sci. Paris, 333 (2001) 201-207.

[41] Maurin JC, Guiraud R., Relationships between tectonics and sedimentation in the Barremo-Aptian intracontinental basins of Northern Cameroon., J. Afr. Earth Sci., 10(1990) 331-340.
[42] Maurin JC, Guiraud R ., Basement control in the development of the Early Cretaceous West and Central African Rift System. Tectonophy. 228 (1993) 81-95.
[43] Toteu SF, Michard A, Bertrand JM, Rocci, G U-Pb Dating of Precambrian Rocks from Northern Cameroon, Orogenic Evolution and Chronology of Pan-African Belt of Central Africa. Precambrian Res. 37 (1987) 71-87. https://doi.org/10.1016/0301-9268(87)90040-4
[44] Taylor SR, McLennan SM., The continental crust: Its composition and evolution. Blackwell, Oxford, (1985) 312.
[45] Haskin LA, Haskin MA, Frey FA, Wildman TR Relative and absolute terrestrial abundances of the rare piles of earth. In: Ahrens, L.H. (Ed.), Origin and distribution of the elements. Oxford: Pergamon, (1968) 889-912.
[46] Eltom HA, Abdullatif OM, Makkawi MH., Rare earth element geochemistry of shallow carbonate outcropping strata in Saudi Arabia: application for depositional environments prediction. Sediment. Geol. 348(2017) 51-68.
[47] Allègre C, Michard G., Introduction to Geochemistry (Geophysics and Astrophysics Monographs). 10, D. Reidel Publishing Company, Boston, USA, 143(1974).
[48] Floyd PA, Leveridge BE., Tectonic environment of the Devonian Gramscatho basin, South Cornwall: framework mode and geochemical evidence from turbidite sandstones. J. Geol. Soc.144(1987) 531-542.
[49] Etemad-Saeed N, Hosseini-Barzi M, Armstrong-Altrin JS (2011) Petrography and geochemistry of clastic sedimentary rocks as evidence for the provenance of the Lower Cambrian Lalun Formation, Posht-e-badam block, central Iran. J. Afr. Earth Sci. 61(1987) 142-159.
[50] Nagarajan R, Armstrong-Altrin JS, Nagendra R, Madhavaraju J, Moutte J., Petrography and geochemistry of terrigenous sedimentary rocks in the Neoproterozoic Rabanpalli formation, Bhima Basin, northern Karnataka, Southern India: implications for paleoweathering condition, provenance, and source rocks composition. J. Geol. Soc. India, 70(2007) 297-312.
[51] Ngueutchoua G, Eyong TJ, Ekoa-Bessa AZ, Agheenwi ABZ, Maschouer EA, Kemteu SC, Dzoti LY, Hamadou T, Baboule MOB, Nguemo KG Provenance and depositional history of Mesozoic sediments from the Mamfe basin and Douala sub-basin (SW Cameroon) unraveled by geochemical analysis, J. Afr. Earth Sci. 158 (2019) 103550.
[52] Garver JI, Royce PR, Smick AT., Chromium and nickel in the shale of the Taconic foreland: a case study for the provenance of fine-grained sediments with an ultramafic source. J. Sediment. Res. 100 (1996) 100-106.
[53] Cullers RL., Mineralogical and chemical changes of soil and stream sediment formed by intense weathering of the Danburg granite, Georgia, U.S.A. Lithos, 21(1988) 301-314.
[54] Ganwa AA, Frisch W, Siebel W, Ekodeck EG, Shang, KC, Ngako V., Archean inheritances in the pyroxene-amphibole-bearing gneiss of the Méiganga Area (Central North Cameroon): Geochemical and $^{207}Pb/^{206}Pb$ age imprints. C. R. Geosci. 340 (2008) 211-222.
[55] Ganwa AA, Klotzli SU, Hauzenberger C Evidence for Archean inheritance in the pre-Panafrican crust of Central Cameroon: Insight from internal zircon structure and LA-MC-ICP-MS U-Pb ages. J. Afr. Earth Sci. 120 (2016) 12-22.
[56] Hatch JR, Leventhal JS., Relationship between inferred redox potential of the depositional environment and geochemistry of the Upper Pennsylvanian (Missourian) stark shale member of the Dennis Limestone, Wabaunsee County, Kansas, USA. Chem. Geol. 99(1992) 65-82.
[57] Jones B, Manning DAC., Comparison of geochemical indices used for the interpretation of palaeoredox conditions in ancient mudstones. Chem. Geol. 111(1994) 111-129.
[58] Mao LJ, Mo DW, Yang JH, Guo YY, Lv HY Rare earth elements geochemistry in surface floodplain sediments from the Xiangjiang River, the middle reach of Changjiang River, China. Quater. Int. 336 (2014) 80-88.
[59] Zhao BS, Li RX, Wang XZ, Wu XY, Wang N, Qin, XL, Cheng JH, Li JJ ., Sedimentary environment and preservation conditions of organic matter analysis of Shanxi formation mud dshale in Yanchang exploration area, Ordos Basin. Geol Sci Technol Inf ((in Chinese with English abstract), 35(6) (2016) 103-111.
[60] Xu QL, Liu B, Ma YS, Song XM, Wang YJ, Chen ZX., Geological and geochemical characterization of lacustrine shale: A case study of the Jurassic Da'anzhai member shale in the central Sichuan Basin, southwest China. J. Nat. Gas Sci. Eng. 47 (2017) 124-139.
[61] Teng GE, Hui LW, Xu YC, Chen JF ., Correlative study on parameters of inorganic geochemistry and hydrocarbon source rocks formative environment. Adv. Earth Sci. (in Chinese with English abstract), 20(2) (2005) 193-200.
[62] Roy DK, Roser BP., Climatic control on the composition of Carboniferous-Permian Gondwana sediments, Khalaspir basin, Bangladesh. Gondwana Res. 23 (2013) 1163-1171.
[63] Sarki-Yandoka BM, Abdullah WH, Abubakar MB, Hakimi MH, Adegoke AK., Geochemical characterization of Early Cretaceous lacustrine sediments of Bima Formation, Yola sub-basin, Northern Benue trough, NE Nigeria: Organic matter input, preservation, paleoenvironment and palaeoclimatic conditions. Mar. Petrol. Geol. 61 (2015) 82-94.
[64] Wang YY, Wu P., Geochemical criteria of sediments in the coastal area of Jiangsu and Zhejiang Provinces. J Tongji Univ (Nat Sci) (in Chinese with English abstract) 4 (1983) 82-90.
[65] Ndjigui JD, Onana LV, Sababa E, Bayiga CE Mineralogy and geochemistry of the Lokoundje alluvial clays from the Kribi deposits, Cameroonian Atlantic coast: Implications for their origin and depositional environment. J. Afr. Earth Sci.143 (2018) 102-117.
[66] Cullers RL., The chemical signature of source rocks in size fractions of Holocene stream sediment derived from metamorphic rocks in the Wet Mountains region, Colorado, U.S.A. Chem. Geol. 113 (1994) 317-343.
[67] Teng GE, Liu WH, Xu YC., Identification of effective source rocks of Ordovician marine sediments in Ordos Basin. Prog. Nat. Sci. (in Chinese), 14(11) (2004) 1249-1252.
[68] Liu J, Yao YB, Elsworth D, Pan ZJ, Sun XX, Ao WH., Sedimentary characteristics of the Lower Cambrian Niutitang shale in the southeast margin of Sichuan Basin, China. J. Nat. Gas Sci. Eng. 36 (2016) 1140-1150.
[69] Cullers RL, Podkovyrov NV., Geochemistry of the Mesoproterozoic Lakhanda shales in southeastern Yakutia, Russia: Implications for mineralogical and provenance control, and recycling. Precambrian Res.104(2000) 77-93.